A coupled model for train-track-bridge stochastic analysis with consideration of spatial variation and temporal evolution

Xu, Lei; Zhai, Wanming; Li, Zili

DOI
10.1016/j.apm.2018.07.001

Publication date
2018

Document Version
Final published version

Published in
Applied Mathematical Modelling

Applied Mathematical Modelling 63 (2018) 709–731

Contents lists available at ScienceDirect

Applied Mathematical Modelling

journal homepage: www.elsevier.com/locate/apm

A coupled model for train-track-bridge stochastic analysis with consideration of spatial variation and temporal evolution

Lei Xu[a,b,*], Wanming Zhai[a], Zili Li[b]

[a] Train and track research institute, State-Key Laboratory of Traction Power, Southwest Jiaotong University, Chengdu 610031, China
[b] The Section of Road and Railway Engineering, Delft University of Technology, Delft 2628, The Netherlands

ARTICLE INFO

Article history:
Received 30 September 2017
Revised 2 June 2018
Accepted 4 July 2018
Available online 29 July 2018

Keywords:
Train-track-bridge interactions
Random vibrations
Monte-Carlo method
Karhunen–Loève expansion
Track irregularities

ABSTRACT

Due to random characteristics of system parameters and excitations, the dynamic assessment and prediction for the train-track-bridge interaction systems become rather complex issues needing to be addressed, especially considering the longitudinal inhomogeneity and uncertainty of dynamic properties in physics and correspondingly their temporal evolutions. In this paper, a temporal-spatial coupled model is developed to fully deal with the deterministically/non-deterministically computational and analytical matters in the train-track-bridge interactions with a novelty, where a train-track-bridge interaction model is newly developed by effectively coupling the three-dimensional nonlinear wheel-rail contact model and the finite element theory, moreover, the Monte-Carlo method (MCM) and Karhunen–Loève expansion (KLE) are effectively united to model the random field of track-bridge systems, and a spectral evolution method accompanied by a track irregularity probabilistic model are introduced to select the most representative track irregularity sets and to characterize their random evolutions in temporal dimension. In terms of random vibration analysis, the high-efficiency and effectiveness of this developed model is validated by comparing to a robust method, i.e., MCM. Apart from validations, multi-applications of the temporal-spatial coupled model from aspects of deterministic computation, random vibration, resonant analysis and long-term dynamic prediction, etc., have been fully presented to illustrate the universality of the proposed model.

1. Introduction

Railway bridges, as a kind of infrastructure, are becoming increasingly important in supporting and guiding the train-track systems. Especially in high-speed lines, the proportion of bridges is much higher than common railway lines that are mainly supported by the subgrade layer. To specific lines, even 90% over is occupied by bridges for conservation of land and environment protection. Hence the theoretical methods and applied technologies related to the assessment of dynamic performance of railway systems, when a train passes through the track/bridge structures, have attracted more and more attentions in last two decades.

Comparing to expensively experimental studies in situ or lab, the dynamic simulations actualized by the computer program have become a dominant strategy in most situations. Till now, the dynamic models developed to characterize the train-track-bridge interactions are numerous, but mostly concentrated on vertical vibrations [1–8], obviously, it limits the re-

* Corresponding author at: Train and track research institute, State-Key Laboratory of Traction Power, Southwest Jiaotong University, Chengdu 610031, China.
E-mail address: leix_2014@my.swjtu.edu.cn (L. Xu).

https://doi.org/10.1016/j.apm.2018.07.001
0307-904X/

Nomenclature

m_{r}	the rail mass per unit length
A_{r}	the cross-sectional area of the rail
W_{r}	the polar moment of inertia of the rail cross-section
L	the length of the beam element
l_{r}	the distance between two adjacent rail pads
E_{r}	the Young's modulus of the rail
(I_{ry},I_{rz})	the flexural moment of inertia about the Y-axis and Z-axis of the cross section of the rail respectively
k_{rt}	the torsional rigidity of the rail cross section around the X-axis
m_{s}	the mass of the slab per unit volume
$(h_{\mathrm{s}},b_{\mathrm{s}},l_{\mathrm{s}})$	the height, width and length of the slab track element respectively
E_{s}	the Young's modulus of the slab track
μ_{s}	the Poisson ratio of the slab track
I_{sz}	the moment of inertia of the track slab around Z-axis
m_p	the mass of the pier
(k_{px},k_{px},k_{px})	the supporting stiffness coefficients of the subgrade in X-, Y- and Z- axis, respectively
(c_{px},c_{px},c_{px})	the supporting damping coefficients of the subgrade in X-, Y- and Z- axis, respectively
$(k_{\mathrm{rp},z},k_{\mathrm{rp},y})$	the vertical and lateral stiffness of the rail pad respectively
$(c_{\mathrm{rp},z},c_{\mathrm{rp},y})$	the vertical and lateral damping of the rail pad respectively
b	the lateral distance between the contact point of rail pad-slab track and the left-side border of the slab along X-axis
$(k_{\mathrm{ca},z},k_{\mathrm{ca},y})$	the vertical and lateral stiffness coefficients of the CAM
$(B_{\mathrm{r}},H_{\mathrm{r}})$	the central lateral and vertical distances between the slab track and the girder
$(k_{\mathrm{p},z},k_{\mathrm{p},y})$	the vertical and lateral stiffness reflecting the properties of the bearing
a_0	the half of the horizontal distance between two contact points
$(r_{\mathrm{li}},r_{\mathrm{ri}})$	the rolling radius of the left and right wheelset respectively
Ω	the nominal rolling angular velocity of the wheelset
(I_{wY},I_{wZ})	the moment of inertia of the wheelset around Y- and Z- axis
M_w	the mass of the wheelset
R_i	the radius of the curvature of the rail corresponding to the ith wheelset
ϕ_{wi}	the angle of superelevation corresponding to the center of the ith wheelset
$(\dot{\varphi}_{wi},\ \ddot{\varphi}_{wi})$	the first-order and second-order derivatives of ϕ_i
r_0	the nominal rolling radius of the wheelset
$\dot{\lambda}_{wi}$	the first-order derivative of the curvature
$\bar{g}$	the acceleration of gravity
V	the running speed of the vehicle
M_{c}	the mass of the car body
(I_{cX},I_{cZ})	the moment of inertia of the car body around X- and Z- axis respectively
R_{c}	the radius of curvature with regard to the centroid of the car body
ϕ_{c}	the angle of superelevation corresponding to the centroid of the car body
$\ddot{\varphi}_c$	the second-order derivative of ϕ_{c}
$\dot{\varsigma}_c$	the first-order derivative of the track curvature
H_{tw}	the vertical distance between the centroid of the bogie frame and the center of the wheelset
H_{bt}	the vertical distance between the centroid of the bogie frame and the bottom plane of the secondary suspension
H_{cb}	the vertical distance between the centroid of the bogie frame and the upper plane of the secondary suspension
$(k_{\mathrm{sz}},k_{\mathrm{sy}},k_{\mathrm{sx}})$	the secondary suspension stiffness in vertical, lateral and longitudinal directions
$(k_{\mathrm{pz}},k_{\mathrm{py}},k_{\mathrm{px}})$	the primary suspension stiffness in vertical, lateral and longitudinal directions
$(d_{\mathrm{s}},d_{\mathrm{p}})$	the semi-horizontal distance of the secondary and primary suspension respectively
l_{c}	the semi-longitudinal distance between bogies
l_{t}	the semi-longitudinal distance between wheelsets in a bogie
(l_h,l_v)	the lateral and vertical distance between the wheel-rail contact point and the centroid of the rail

search scopes since the issues on lateral stability and safety of system components have gradually become notable concerns in railway engineering, especially in conditions of high speed operations. Accounting for this, more and more researchers start to focus on building the three-dimensional train-track/bridge interaction models, see for example, Zhai et al. [9] made a pioneering work in comprehensively considering the coupled dynamics between a vehicle and the tracks, in which the

three-dimensional (3-D) nonlinear contact/creep in wheel-rail interactions are introduced in focused manner, later, by adopting the same fundamentals, extensive researches in train-track-bridge coupled dynamics are put into practice [10,11]; moreover, Refs. [12–17] conducted significant work on 3-D train-bridge interactions, but neglecting the effects of track structural participations on synthetic vibrations, additionally, only linear wheel-rail interactions are accounted for; Zeng et al. [18] constructed a rather comprehensive model for train-slab track-bridge interactions, but still, the core mechanism highlighting the complex wheel-rail interactions is linearized to unify the system components by energy-variational principle [19].

Apart from the developments on constructing train-bridge dynamic simulation models, researchers gradually extend the general deterministic computations into random vibration analysis in light of the random characteristics of the train/track/bridge systems on physical properties and mechanical status. With regard to the random analysis of train-track/bridge interactions, there are mainly three types of methods, i.e., Monte-Carlo method (MCM) [6,20,21], pseudo-excitation method (PEM) [17,18,22,23] and probability density evolution method (PDEM) [16,24], where the system parameters or excitations, e.g, track irregularities and seismic motions, etc., are assumed to be random processes statically characterized by probability density function (PDF) and spectral densities. Undoubtedly, these work has taken significant steps towards the road of random analysis, however, far more scientific researches need to be probed into, e.g.,

- Random simulation involving with the longitudinal uncertainty of dynamic properties of track/bridge systems at spatial dimension. Though fragmentary reports investigating the effects of random track bed stiffness on vehicle-track interactions have been presented [25], a united and high-efficient method dealing with random simulation and combination of multiple variables is rarely presented;
- Ergodic characterization of the system excitations. For example, track irregularities, perhaps the most important excitation of train-track/bridge systems, hold random nature. In Refs. [16,18], only the excitation of specific track irregularity spectrums, which are just statistical status of the rail deformation at one probability, is considered, certainly, based on which the full responses of system components cannot be revealed;
- The strategies to characterize the evolution of system dynamic characteristics affecting the long-term behaviors of train-track/bridge systems.

Previously, Xu and Zhai [26] had proposed a theoretical prototype to expand the general random vibration analysis into temporal-spatial stochastic analysis with respect to the vehicle-track systems, in which the randomness and correlation between longitudinal system parameters are considered but being limited to normal distribution, moreover, the ergodic simulation of track random irregularities are solved by a probabilistic method. This research notices the features of railway lines in large-scale construction and longitudinal unevenness/randomness in system parameters and track irregularities, the temporal-spatial stochastic model is therefore established to wholly consider the possibility of combination over system parameters and excitations, and achieving far more comprehensive dynamics results that are necessities in reliability assessment, track maintenance and design, etc.

Based on the fundamentals of the work in Ref. [26], the studies aiming at constructing a general model for achieving the temporal-stochastic analysis of train-track-bridge systems will be further extended and perfected. The main content of this paper can be illustrated by: firstly, a more advanced 3-D nonlinear train-track-bridge dynamic model will be developed by fully modelling the tracks and the bridges as an integrated one, while the interactions between the train and the track-bridge systems are characterized by the complex nonlinear wheel-rail forces by correcting the deficiency of Ref. [18,27]; secondly, a united method will be provided to randomly simulate the system variables that are correlated and following arbitrary probability distribution, based on MCM and Karhunen–Loève expansion (KLE); thirdly, a statistical strategy is developed to describe the evolution of track random irregularities accompanied by a simple introduction of the track irregularity probabilistic model; fourthly, the theoretical framework for constructing the temporal-spatial stochastic model for train-track-bridge interactions is presented; finally, numerical studies and conclusions will be further presented.

2. Modelling for train-track-bridge interactions

2.1. Basic instructions

To the three-dimensional (3-D) train-track-bridge model (Fig. 1), the following instructions should be made in advance, namely

(1) The train consists of the front and rear motor car and several trailer cars modelled as rigid bodies of a car body, two bogie frame, four wheelsets and linear suspension systems, and the vehicles move at a constant velocity V along the tracks;
(2) The bridge is modelled as simply supported girder bridges; the tracks resting on the bridges are chosen as slab tracks modelled by thin-plate element, while the tracks on rigid-subgrades are modelled by commonly used ballasted tracks.
(3) Only the presentation over the dynamic equations of motion for the train-track-bridge interactions will be illustrated for brevity.

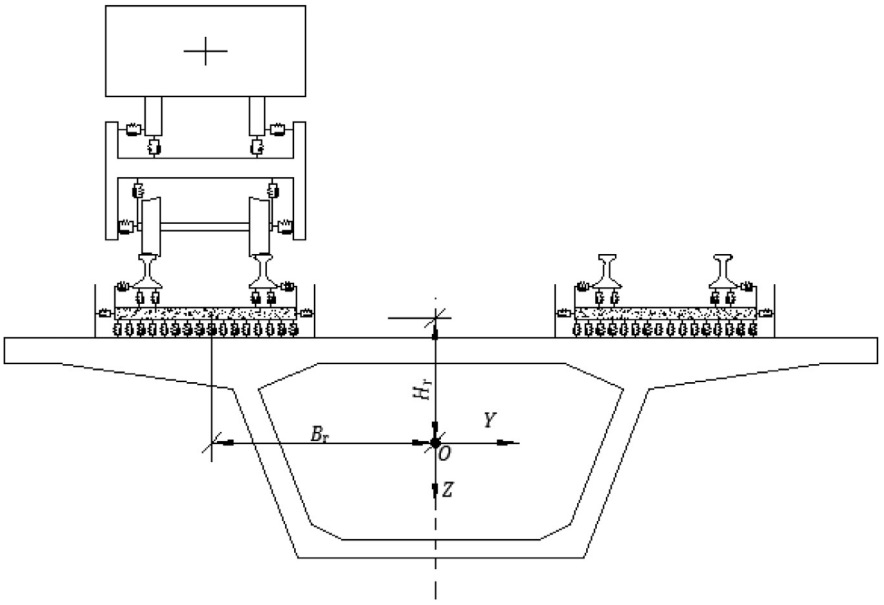

Fig. 1. Three-dimensional train-track-bridge interaction model (end view).

2.2. Dynamic equations of motion for train-track-bridge interactions

Based on fundamentals of finite element theory and energy-variational principle, one can derive the 3-D equations of motion in sub-matrix form for the train-track bridge interaction system as

$$\begin{bmatrix} \boldsymbol{M}_{tt} & 0 & 0 & 0 & 0 \\ 0 & \boldsymbol{M}_{rr} & 0 & 0 & 0 \\ 0 & 0 & \boldsymbol{M}_{ss} & 0 & 0 \\ 0 & 0 & 0 & \boldsymbol{M}_{bb} & 0 \\ 0 & 0 & 0 & 0 & \boldsymbol{M}_{pp} \end{bmatrix} \begin{bmatrix} \ddot{\boldsymbol{X}}_t \\ \ddot{\boldsymbol{X}}_r \\ \ddot{\boldsymbol{X}}_s \\ \ddot{\boldsymbol{X}}_b \\ \ddot{\boldsymbol{X}}_p \end{bmatrix} + \begin{bmatrix} \boldsymbol{C}_{tt} & \boldsymbol{C}_{tr} & 0 & 0 & 0 \\ \boldsymbol{C}_{rt} & \boldsymbol{C}_{rr} & \boldsymbol{C}_{rs} & 0 & 0 \\ 0 & \boldsymbol{C}_{rs} & \boldsymbol{C}_{ss} & \boldsymbol{C}_{sb} & 0 \\ 0 & 0 & \boldsymbol{C}_{bs} & \boldsymbol{C}_{bb} & \boldsymbol{C}_{bp} \\ 0 & 0 & 0 & \boldsymbol{C}_{pb} & \boldsymbol{C}_{pp} \end{bmatrix} \begin{bmatrix} \dot{\boldsymbol{X}}_t \\ \dot{\boldsymbol{X}}_r \\ \dot{\boldsymbol{X}}_s \\ \dot{\boldsymbol{X}}_b \\ \dot{\boldsymbol{X}}_p \end{bmatrix}$$
$$+ \begin{bmatrix} \boldsymbol{K}_{tt} & \boldsymbol{K}_{tr} & 0 & 0 & 0 \\ \boldsymbol{K}_{rt} & \boldsymbol{K}_{rr} & \boldsymbol{K}_{rs} & 0 & 0 \\ 0 & \boldsymbol{K}_{rs} & \boldsymbol{K}_{ss} & \boldsymbol{K}_{sb} & 0 \\ 0 & 0 & \boldsymbol{K}_{bs} & \boldsymbol{K}_{bb} & \boldsymbol{K}_{bp} \\ 0 & 0 & 0 & \boldsymbol{K}_{pb} & \boldsymbol{K}_{pp} \end{bmatrix} \begin{bmatrix} \boldsymbol{X}_t \\ \boldsymbol{X}_r \\ \boldsymbol{X}_s \\ \boldsymbol{X}_b \\ \boldsymbol{X}_p \end{bmatrix} = \begin{bmatrix} \boldsymbol{F}_t \\ \boldsymbol{F}_r \\ \boldsymbol{F}_s \\ \boldsymbol{F}_b \\ \boldsymbol{F}_p \end{bmatrix} \tag{1}$$

where the subscripts "*t*", "*r*", "*s*", "*b*" and "*p*" denote the train, rail, slab track, girder and pier, respectively.

2.2.1. The methodologies used to couple the train-track-bridge systems

Surveying this train-track-bridge coupled system, one can discover that the connection of all system components including the wheel-rail interfacial interaction can be equivalently treated as a form of spring-dashpot contact.

Obviously the dynamic problems of elastic systems can be also transformed as static equilibrium problems where d' Alembert principle and the effects of damping forces is respectively introduced and considered by a general form [19]

$$\boldsymbol{f}_e = \boldsymbol{f}_\rho + \boldsymbol{f}_c - \boldsymbol{F}\mathrm{sign}(\boldsymbol{u}) + \boldsymbol{p}(t) + \boldsymbol{G} \tag{2}$$

with $\boldsymbol{f}_\rho = \int_\upsilon (-\rho\ddot{\boldsymbol{u}})\mathrm{d}\upsilon$; $\boldsymbol{f}_c = \int_\upsilon (-c\dot{\boldsymbol{u}})\mathrm{d}\upsilon$,where $\boldsymbol{f}_e$, $\boldsymbol{f}_\rho$, $\boldsymbol{f}_c$, $\boldsymbol{F}$, $\boldsymbol{p}(t)$ and $\boldsymbol{G}$ are the vectors of system elastic force, inertia force, damping force, Coulomb's friction force, external interfere force and gravity, respectively; $\ddot{\boldsymbol{u}}$, $\dot{\boldsymbol{u}}$ and $\boldsymbol{u}$ are respectively the acceleration, velocity and displacement quantity; ρ and c respectively denote the parameters of mass density and damping coefficient.

Based on the principle of virtual work, the equation below can be derived by accounting for the system virtual displacement $\delta\boldsymbol{u}$, that is [19]

$$\delta U_e = -\int_\upsilon \delta\boldsymbol{u}^{\mathrm{T}}\rho\ddot{\boldsymbol{u}}\mathrm{d}\upsilon - \int_\upsilon \delta\boldsymbol{u}^{\mathrm{T}}c\dot{\boldsymbol{u}}\mathrm{d}\upsilon - \delta\boldsymbol{u}^{\mathrm{T}}\boldsymbol{F}\mathrm{sign}(\boldsymbol{u}) + \delta\boldsymbol{u}^{\mathrm{T}}\boldsymbol{p}(t) + \delta\boldsymbol{u}^{\mathrm{T}}\boldsymbol{G} \tag{3}$$

with $U_\rho = \int_\upsilon \delta\boldsymbol{u}^{\mathrm{T}}\rho\ddot{\boldsymbol{u}}\mathrm{d}\upsilon$, $U_c = \int_\upsilon \delta\boldsymbol{u}^{\mathrm{T}}c\dot{\boldsymbol{u}}\mathrm{d}\upsilon$, $V_F = \boldsymbol{u}^{\mathrm{T}}\boldsymbol{F}\mathrm{sign}(\boldsymbol{u})$, $V_p = -\boldsymbol{u}^{\mathrm{T}}\boldsymbol{p}(t)$, $V_g = -\boldsymbol{u}^{\mathrm{T}}\mathbf{G}$, in which U_e is the elastic strain energy of the systems; U_ρ, U_c, V_F and V_p are the negative work of the non-potential forces, that is, the system inertia force, damping

force, Coulomb's friction force and external interfere force, respectively; V_g is the gravitational potential energy of the systems.

Following the principle of finite element method (FEM), it is known that $\boldsymbol{u}=\mathrm{N}\boldsymbol{X}$, $\dot{\boldsymbol{u}}=\mathrm{N}\dot{\boldsymbol{X}}$ and $\ddot{\boldsymbol{u}}=\mathrm{N}\ddot{\boldsymbol{X}}$, in which N is the equivalent shape function, $\boldsymbol{X}$, $\dot{\boldsymbol{X}}$ and $\ddot{\boldsymbol{X}}$ are respectively the displacement, velocity and acceleration vector of the systems, thus Eq. (3) can be transformed as

$$\delta U_e+\delta\boldsymbol{X}^{\mathrm{T}}\boldsymbol{M}\ddot{\boldsymbol{X}}+\delta\boldsymbol{X}^{\mathrm{T}}\boldsymbol{C}\dot{\boldsymbol{X}}=\delta\boldsymbol{X}^{\mathrm{T}}\boldsymbol{F}_s \tag{4}$$

with $\boldsymbol{M}=\int_\upsilon \rho\mathrm{N}_m^{\mathrm{T}}\mathrm{N}_m\mathrm{d}\upsilon$, $\boldsymbol{C}=\int_\upsilon c\mathrm{N}_c^{\mathrm{T}}\mathrm{N}_c\mathrm{d}\upsilon$, $\boldsymbol{F}_s=-\mathrm{N}_F^{\mathrm{T}}\boldsymbol{F}\mathrm{sign}(\mathrm{N}_F\boldsymbol{X})-\mathrm{N}_p^{\mathrm{T}}\boldsymbol{p}(t)-\mathrm{N}_G^{\mathrm{T}}\boldsymbol{G}$, where N_m and N_c denote the equivalent shape functions for the mass matrix and damping matrix respectively; N_F, N_p and N_G denote the equivalent shape functions for load distribution; δU_e is the variation of the elastic strain energy, which has different expressions according to the motion modes, for example, $\delta U_e=\delta\boldsymbol{X}^{\mathrm{T}}\int_\upsilon EI\mathrm{N}^{''\mathrm{T}}\mathrm{N}^{''}\mathrm{d}\upsilon\ddot{\boldsymbol{X}}$ for the elastic deformation energy of a beam, in which E and I denote the modulus of elasticity and moment of inertia respectively, $\mathrm{N}^{''}$ denotes the second derivative of the equivalent shape function.

From Eq. (4) one can observe that the dynamic matrices can be obtained by removing the virtual displacement term $\delta\boldsymbol{X}$, thus the key work in building the equations of motion for a dynamical system lies in clarifying the shape functions and loading vectors. The detail methodology and derivation process from the potential energy of a dynamic system to the correspondingly dynamic matrices have been presented in the work of Xu et al. [28], which can be consulted for reference.

In the following parts, the displacement vectors and sub-matrices will be given directly without further derivations for brevity.

2.2.2. Displacement vector

The total train displacement vector, $\boldsymbol{X}_t$, can be assembled as

$$\boldsymbol{X}_t=\begin{bmatrix}\boldsymbol{X}_{Mo,1} & \boldsymbol{X}_{Tr,1} & \boldsymbol{X}_{Tr,2} & \dots & \boldsymbol{X}_{Tr,N_v} & \boldsymbol{X}_{Mo,2}\end{bmatrix}^{\mathrm{T}} \tag{5}$$

where the superscript "T" denotes the transposition of the matrix; the subscripts "*Mo*", "*Tr*" denote the motor car and trailer car respectively, and $\boldsymbol{X}_{Mo,i}$, $i=1, 2$ and $\boldsymbol{X}_{Tr,j}$, $j=1, 2, ..., N_v$ denote the sub-vectors of the ith motor car and the jth trailer car, all with 35 degrees of freedom (DOF's), as shown in Appendix A-Table A1.

The displacement vector of the rail, $\boldsymbol{X}_r$, with order of $(2\times N_r\times n_r)\times 1$, where N_r is the total number of rail beam element, n_r is the number of DOFs of a rail beam and the number "2" originates from the left- and right- side of the rails, can be written as

$$\boldsymbol{X}_r=\begin{bmatrix}\boldsymbol{X}_{Lr,1} & \boldsymbol{X}_{Lr,2} & \dots & \boldsymbol{X}_{Lr,n_r} & \boldsymbol{X}_{Rr,1} & \boldsymbol{X}_{Rr,2} & \dots & \boldsymbol{X}_{Rr,n_r}\end{bmatrix}^{\mathrm{T}} \tag{6}$$

where the subscript "*Lr*" and "*Rr*" denotes the left- and right-side rail respectively. The DOF for each node of the rail beam element has been listed in Appendix A-Table A2.

The displacement vector of the slab track, $\boldsymbol{X}_s$, with order of $(N_s\times n_s)\times 1$, where N_s is the total number of slab element, n_s is the number of DOFs of a slab thin-plate element, can be written as

$$\boldsymbol{X}_s=\begin{bmatrix}\boldsymbol{X}_{s,1} & \boldsymbol{X}_{s,2} & \dots & \boldsymbol{X}_{s,N_s}\end{bmatrix}^{\mathrm{T}} \tag{7}$$

where the $\boldsymbol{X}_{s,l}$, $l=1, 2, ..., N_s$, denotes the displacement vector of the lth slab track element. The DOFs for the thin-plate element of the slab tracks have been listed in Appendix A-Table A3.

The displacement vector of the girder, $\boldsymbol{X}_b$, with order of $(N_b\times n_b)\times 1$, where N_b is the total number of bridge girder elements, n_b is the number of DOFs of a girder element, can be written as

$$\boldsymbol{X}_b=\begin{bmatrix}\boldsymbol{X}_{b,1} & \boldsymbol{X}_{b,2} & \dots & \boldsymbol{X}_{b,N_b}\end{bmatrix}^{\mathrm{T}} \tag{8}$$

where the $\boldsymbol{X}_{b,k}$, $k=1, 2, ..., N_b$ denotes the displacement vector of the kth girder element. The DOFs for the girder element are the same as the rail beam element.

The displacement vector of the pier, $\boldsymbol{X}_p$, with order of $(N_p\times n_p)\times 1$, where N_p is the total number of bridge girder elements, n_p is the number of DOFs of a girder element, can be written as

$$\boldsymbol{X}_p=\begin{bmatrix}\boldsymbol{X}_{p,1} & \boldsymbol{X}_{p,2} & \dots & \boldsymbol{X}_{p,N_b}\end{bmatrix}^{\mathrm{T}} \tag{9}$$

where the $\boldsymbol{X}_{p,q}$, $q=1, 2, ..., N_p$ denotes the displacement vector of the qth girder element. The DOFs for the pier element are linear displacements along *X*-, *Y*- and *Z*- axis since being assumed as mass element.

2.2.3. Sub-matrices for the train

The mass matrix of the train, $\boldsymbol{M}_{tt}$, can be assembled as

$$\begin{aligned}\boldsymbol{M}_{tt}=&\sum_{Tr=1}^{N_v}\boldsymbol{M}_{Tr,\mathrm{c}}(\boldsymbol{\Theta}_{Tr,\mathrm{c}},\boldsymbol{\Theta}_{Tr,\mathrm{c}})+\boldsymbol{M}_{Tr,\mathrm{Gq}}(\boldsymbol{\Theta}_{Tr,\mathrm{Gq}},\boldsymbol{\Theta}_{Tr,\mathrm{Gq}})+\boldsymbol{M}_{Tr,\mathrm{Gh}}(\boldsymbol{\Theta}_{Tr,\mathrm{Gh}},\boldsymbol{\Theta}_{Tr,\mathrm{Gh}})+\sum_{i=1}^{n_{\mathrm{wr}}}\boldsymbol{M}_{Tr,\mathrm{w},i}(\boldsymbol{\Theta}_{Tr,\mathrm{w},i},\boldsymbol{\Theta}_{Tr,\mathrm{w},i})\\&+\sum_{Mo=1}^{2}\boldsymbol{M}_{Mo,\mathrm{c}}(\boldsymbol{\Theta}_{Mo,\mathrm{c}},\boldsymbol{\Theta}_{Mo,\mathrm{c}})+\boldsymbol{M}_{Mo,\mathrm{Gq}}(\boldsymbol{\Theta}_{Mo,\mathrm{Gq}},\boldsymbol{\Theta}_{Mo,\mathrm{Gq}})\end{aligned}$$

$$+\boldsymbol{M}_{Mo,\mathrm{Gh}}(\boldsymbol{\Theta}_{Mo,\mathrm{Gh}},\boldsymbol{\Theta}_{Mo,\mathrm{Gh}})+\sum_{i=1}^{n_{\mathrm{wr}}}\boldsymbol{M}_{Mo,\mathrm{w},i}(\boldsymbol{\Theta}_{Mo,\mathrm{w},i},\boldsymbol{\Theta}_{Mo,\mathrm{w},i}) \tag{10}$$

with

$$\boldsymbol{\Theta}_u=\begin{bmatrix}y_u & z_u & \psi_u & \beta_u & \phi_u\end{bmatrix},$$
$$\boldsymbol{M}_u(\boldsymbol{\Theta}_u,\boldsymbol{\Theta}_u)=\mathrm{diag}([m_u \quad m_u \quad I_{u,z} \quad I_{u,y} \quad I_{u,x}\ ]),$$
$$\boldsymbol{\Theta}_{\mathrm{w},g}=\begin{bmatrix}y_{\mathrm{w},g} & z_{\mathrm{w},g} & \psi_{\mathrm{w},g} & \beta_{\mathrm{w},g} & \phi_{\mathrm{w},g}\end{bmatrix},$$
$$\boldsymbol{M}_{\mathrm{w},g}(\boldsymbol{\Theta}_{\mathrm{w},g},\boldsymbol{\Theta}_{\mathrm{w},g})=\mathrm{diag}([m_{\mathrm{w},g} \quad m_{\mathrm{w},g} \quad I_{\mathrm{w},z,g} \quad I_{\mathrm{w},y,g} \quad I_{\mathrm{w},x,g}\ ]),$$

where the subscript "u" will be substituted by "c", "Gq" and "Gh" representing the car body, front bogie frame and rear bogie frame respectively; the subscript "w" denotes the wheelset, "g" denotes the gth wheelset; m is the mass, I_x, I_y and I_z denote moment of inertia around X-, Y- and Z- axis; $\boldsymbol{\Theta}[\bullet]$ is a general operator indicating the DOF number corresponding to the matrices.

The stiffness matrix of the train can be derived as

$$\boldsymbol{K}_{tt}=\sum_{Tr=1}^{N_v}\boldsymbol{K}_{Tr}+\sum_{Mo=1}^{2}\boldsymbol{K}_{Mo} \tag{11}$$

The detailed expression of Eq. (11) has been elaborated in Appendix B [29]. Additionally, the damping matrix of the train, $\boldsymbol{C}_{tt}$, has almost the same expression as $\boldsymbol{K}_{tt}$. It is just needed to substitute the stiffness coefficient k with damping coefficient c.

2.2.4. Sub-matrices for the rail

The mass matrix of the rail, $\boldsymbol{M}_{rr}$, can be written as

$$\boldsymbol{M}_{rr}=\sum_{h=1}^{N_r}\sum_{g=1}^{2}m_{\mathrm{r}}\left(\int_0^{l_{\mathrm{r}}}N_{X\mathrm{r}}^{\mathrm{T}}N_{X\mathrm{r}}\mathrm{d}\xi+\int_0^{l_{\mathrm{r}}}N_{Y\mathrm{r}}^{\mathrm{T}}N_{Y\mathrm{r}}\mathrm{d}\xi+\int_0^{l_{\mathrm{r}}}N_{Z\mathrm{r}}^{\mathrm{T}}N_{Z\mathrm{r}}\mathrm{d}\xi+\int_0^{l_{\mathrm{r}}}\frac{W_{\mathrm{r}}}{A_{\mathrm{r}}}N_{\theta_X\mathrm{r}}^{\mathrm{T}}N_{\theta_X\mathrm{r}}\mathrm{d}\xi\right) \tag{12}$$

with

$$N_{X\mathrm{r}}=N_{\theta_X\mathrm{r}}=\begin{bmatrix}\ldots & 1-\xi/L & \ldots & \xi/L & \ldots\end{bmatrix}_{1\times n_r},$$
$$N_{Y\mathrm{r}}=\begin{bmatrix}\ldots & 1-3\left(\frac{\xi}{L}\right)^2+2\left(\frac{\xi}{L}\right)^3 & \left(\frac{\xi}{L}-2\left(\frac{\xi}{L}\right)^2+\left(\frac{\xi}{L}\right)^3\right)L & 3\left(\frac{\xi}{L}\right)^2-2\left(\frac{\xi}{L}\right)^3 & \left(\left(\frac{\xi}{L}\right)^3-\left(\frac{\xi}{L}\right)^2\right)L & \ldots\end{bmatrix}_{1\times n_r},$$
$$N_{Z\mathrm{r}}=\begin{bmatrix}\ldots & 1-3\left(\frac{\xi}{L}\right)^2+2\left(\frac{\xi}{L}\right)^3 & -\left(\frac{\xi}{L}-2\left(\frac{\xi}{L}\right)^2+\left(\frac{\xi}{L}\right)^3\right)L & 3\left(\frac{\xi}{L}\right)^2-2\left(\frac{\xi}{L}\right)^3 & -\left(\left(\frac{\xi}{L}\right)^3-\left(\frac{\xi}{L}\right)^2\right)L & \ldots\end{bmatrix}_{1\times n_r},$$

where $N_{X\mathrm{r}}$, $N_{Y\mathrm{r}}$, $N_{Z\mathrm{r}}$ and $N_{\theta_X\mathrm{r}}$ are the shape functions for displacement along X-, Y- and Z- axis and angle around X –axis; $g=1, 2$ denote the left and right side rail along X-axis; N_r is the total number of rail beam elements; ζ is the local distance from the left node of the rail beam to arbitrary points within the beam element along X-axis.

The stiffness matrix of the rail, $\boldsymbol{K}_{rr}$, can be written as

$$\boldsymbol{K}_{rr}=\sum_{h=1}^{N_r}\begin{bmatrix}\sum_{g=1}^{2}\left[E_{\mathrm{r}}A_{\mathrm{r}}\int_0^{l_{\mathrm{r}}}[N_{X\mathrm{r}}']^{\mathrm{T}}[N_{X\mathrm{r}}']\mathrm{d}\xi+E_{\mathrm{r}}I_{\mathrm{ry}}\int_0^{l_{\mathrm{r}}}[N_{Z\mathrm{r}}'']^{\mathrm{T}}[N_{Z\mathrm{r}}'']\mathrm{d}\xi\right]\\+\sum_{g=1}^{2}\left[E_{\mathrm{r}}I_{\mathrm{rz}}\int_0^{l_{\mathrm{r}}}[N_{Y\mathrm{r}}'']^{\mathrm{T}}[N_{Y\mathrm{r}}'']\mathrm{d}\xi+k_{\mathrm{rt}}\int_0^{l_{\mathrm{r}}}[N_{\theta_X\mathrm{r}}']^{\mathrm{T}}[N_{\theta_X\mathrm{r}}']\mathrm{d}\xi\right]\end{bmatrix} \tag{13}$$

where N' and N'' are the first and second derivative of the shape function respectively.

2.2.5. Sub-matrices for the slab tracks

The mass matrix of the slab track, $\boldsymbol{M}_{ss}$, can be written as

$$\boldsymbol{M}_{ss}=\sum_{h=1}^{N_s}m_{\mathrm{s}}h_{\mathrm{s}}\left(\int_{-b_{\mathrm{s}}/2}^{b_{\mathrm{s}}/2}\int_{-l_{\mathrm{s}}/2}^{l_{\mathrm{s}}/2}N_{Z\mathrm{s}}^{\mathrm{T}}N_{Z\mathrm{s}}\mathrm{d}\xi\,\mathrm{d}\zeta+b_{\mathrm{s}}\int_0^{l_{\mathrm{s}}}N_{Y\mathrm{s}}^{\mathrm{T}}N_{Y\mathrm{s}}\mathrm{d}\xi\right) \tag{14}$$

where ζ is the local coordinate along the Y-axis; $N_{Y\mathrm{s}}$ has the same expression as $N_{Y\mathrm{r}}$, while $N_{Z\mathrm{s}}$ is chosen as the shape function of a rectangular thin-plate element.

The stiffness matrix of the slab track, $\boldsymbol{K}_{ss}$, can be written as

$$\boldsymbol{K}_{ss}=\sum_{h=1}^{N_s}\left[\int_0^{l_{\mathrm{s}}}\int_0^{b_{\mathrm{s}}}\boldsymbol{B}^{\mathrm{T}}\boldsymbol{D}\boldsymbol{B}\mathrm{d}\zeta\,\mathrm{d}\xi\right]+E_sI_{sz}\int_0^{l_{\mathrm{s}}}N_{Zs}''^{\mathrm{T}}N_{Zs}''\mathrm{d}\zeta\,] \tag{15}$$

with

$$\boldsymbol{B}=-\left[\frac{\partial^2N_{Z\mathrm{s}}}{\partial\xi^2};\frac{\partial^2N_{Z\mathrm{s}}}{\partial\zeta^2};\frac{\partial^2N_{Z\mathrm{s}}}{\partial\xi\partial\zeta}\right]^{\mathrm{T}},\ \boldsymbol{D}=\frac{E_{\mathrm{s}}h_{\mathrm{s}}^3}{12(1-\mu_{\mathrm{s}}{}^2)}\begin{bmatrix}1 & \mu_{\mathrm{s}} & 0\\ \mu_{\mathrm{s}} & 1 & 0\\ 0 & 0 & (1-\mu_{\mathrm{s}})/2\end{bmatrix},$$

2.2.6. Sub-matrices for the girder

Because the girder is assumed to be beam element as the rails, thus its sub-matrices have the same expressions as the rail.

To the mass matrices of the girder, $\boldsymbol{M}_{bb}$, one can derive it by substituting the "m_{r}", "A_{r}" and "W_{r}" in Eq. (12) with "m_b", "A_b" and "W_b", namely

$$\boldsymbol{M}_{bb}=\sum_{h=1}^{N_s} m_b\left(\int_0^{l_{\mathrm{r}}} N_{X\mathrm{r}}^{\mathrm{T}}N_{X\mathrm{r}}\mathrm{d}\xi+\int_0^{l_{\mathrm{r}}} N_{Y\mathrm{r}}^{\mathrm{T}}N_{Y\mathrm{r}}\mathrm{d}\xi+\int_0^{l_{\mathrm{r}}} N_{Z\mathrm{r}}^{\mathrm{T}}N_{Z\mathrm{r}}\mathrm{d}\xi+\int_0^{l_{\mathrm{r}}}\frac{W_b}{A_b}N_{\theta_X\mathrm{r}}^{\mathrm{T}}N_{\theta_X\mathrm{r}}\mathrm{d}\xi\right) \tag{16}$$

To the stiffness matrix of the girder, $\boldsymbol{K}_{bb}$, it can be obtained by substituting the "E_{r}", "A_{r}", "I_{ry}", "I_{rz}" and "k_{rt}" in Eq. (13) with "E_b", "A_b", "I_{by}", "I_{bz}" and "k_{bt}", namely

$$\boldsymbol{K}_{bb}=\sum_{h=1}^{N_s}\left[\begin{array}{l}\left[E_bA_b\int_0^{l_{\mathrm{r}}}[N_{X\mathrm{r}}']^{\mathrm{T}}[N_{X\mathrm{r}}']\mathrm{d}\xi+E_bI_{by}\int_0^{l_{\mathrm{r}}}[N_{Z\mathrm{r}}'']^{\mathrm{T}}[N_{Z\mathrm{r}}'']\mathrm{d}\xi\right]\\+\left[E_bI_{bz}\int_0^{l_{\mathrm{r}}}[N_{Y\mathrm{r}}'']^{\mathrm{T}}[N_{Y\mathrm{r}}'']\mathrm{d}\xi+k_{bt}\int_0^{l_{\mathrm{r}}}[N_{\theta_X\mathrm{r}}']^{\mathrm{T}}[N_{\theta_X\mathrm{r}}']\mathrm{d}\xi\right]\end{array}\right] \tag{17}$$

Based on the assumption of Rayleigh damping, the damping matrix $\boldsymbol{C}_{bb}$ can be computed by

$$\boldsymbol{C}_{bb}=\alpha\boldsymbol{M}_{bb}+\beta\boldsymbol{K}_{bb} \tag{18}$$

with $\alpha=2\zeta_b\omega_1\omega_2/(\omega_1+\omega_2)$ and $\beta=2\zeta_b/(\omega_1+\omega_2)$.

Where ζ_b is the damping ratio, ω_1 and ω_2 are the first two circular frequencies of vibration of the girder.

2.2.7. Sub-matrices for the pier

The pier is simplified as mass element, the mass, stiffness and damping matrix of which, $\boldsymbol{M}_{pp}$, $\boldsymbol{K}_{pp}$ and $\boldsymbol{C}_{pp}$, can be written as

$$\boldsymbol{M}_{pp}=\sum_{h=1}^{N_p}\mathrm{diag}([m_p\quad m_p\quad m_p\quad])\tag{19}$$

$$\boldsymbol{K}_{pp}=\sum_{h=1}^{N_p}\mathrm{diag}([k_{px}\quad k_{py}\quad k_{pz}\quad])\tag{20}$$

$$\boldsymbol{C}_{pp}=\sum_{h=1}^{N_p}\mathrm{diag}([c_{px}\quad c_{py}\quad c_{pz}\quad])\tag{21}$$

2.2.8. Sub-matrices for the rail-slab track interactions

The matrices for rail-slab interactions are marked with the subscripts "*rs*" and "*sr*", which are derived by the interactions between the rails and the slab tracks connected by the rail pads.

The stiffness matrix, $\tilde{\boldsymbol{K}}_{r-s}$, with order of $(2\times N_r\times n_r+N_s\times n_s)\times(2\times N_r\times n_r+N_s\times n_s)$, can be written as

$$\tilde{\boldsymbol{K}}_{r-s}=\sum_{h=1}^{2(N_r+1)}\left[\begin{array}{l}k_{\mathrm{rp},z}[([N_{Z\mathrm{r}}]_{\xi=0}^{\mathrm{T}}-[N_{Z\mathrm{s}}]_{\xi=0,\zeta=b}^{\mathrm{T}})([N_{Z\mathrm{r}}]_{\xi=0}-[N_{Z\mathrm{s}}]_{\xi=0,\zeta=b})\\+([N_{Z\mathrm{r}}]_{\xi=0}^{\mathrm{T}}-[N_{Z\mathrm{s}}]_{\xi=0,\zeta=b_s-b}^{\mathrm{T}})([N_{Z\mathrm{r}}]_{\xi=0}-[N_{Z\mathrm{s}}]_{\xi=0,\zeta=b_s-b})]\\+k_{\mathrm{rp},y}[([N_{Y\mathrm{r}}]_{\xi=0}^{\mathrm{T}}-[N_{Y\mathrm{s}}]_{\xi=0}^{\mathrm{T}})([N_{Y\mathrm{r}}]_{\xi=0}-[N_{Y\mathrm{s}}]_{\xi=0})]\end{array}\right] \tag{22}$$

The damping matrix $\tilde{\boldsymbol{C}}_{r-s}$ can be obtained by substituting the stiffness coefficients $k_{\mathrm{rp},z}$ and $k_{\mathrm{rp},y}$ in $\tilde{\boldsymbol{K}}_{r-s}$ with damping coefficients $c_{\mathrm{rp},z}$ and $c_{\mathrm{rp},y}$.

It should be noted that the matrices of stiffness and damping are actually assembled ones, which will be further partitioned as

$$\left[\begin{array}{ll}\bar{\boldsymbol{K}}_{rr} & \boldsymbol{K}_{rs}\\ \boldsymbol{K}_{sr} & \bar{\boldsymbol{K}}_{ss,1}\end{array}\right]=\tilde{\boldsymbol{K}}_{r-s},\ \left[\begin{array}{ll}\bar{\boldsymbol{C}}_{rr} & \boldsymbol{C}_{rs}\\ \boldsymbol{C}_{sr} & \bar{\boldsymbol{C}}_{ss1}\end{array}\right]=\tilde{\boldsymbol{C}}_{r-s}, \tag{23}$$

Thus the stiffness and damping matrix of the rail will be replaced by $\boldsymbol{K}_{rr}+\bar{\boldsymbol{K}}_{rr}$ and $\boldsymbol{C}_{rr}+\bar{\boldsymbol{C}}_{rr}$.

2.2.9. Sub-matrices for the slab track-girder interactions

The matrices for slab track-girder interactions are marked with the subscripts "*sb*" and "*bs*", which are derived by the interactions between the slab tracks and the girder connected by the cement asphalt mortar (CAM).

The stiffness matrix, $\tilde{\boldsymbol{K}}_{s-b}$, with order of $(N_s\times n_s+N_b\times n_b)\times(N_s\times n_s+N_b\times n_b)$, can be written as

$$\tilde{\boldsymbol{K}}_{s-b}=\sum_{h=1}^{N_s}\left[k_{\mathrm{ca},z}\int_0^{l_s}\int_0^{b_s}N_{Z,sb}^{\mathrm{T}}N_{Z,sb}\mathrm{d}\zeta\,\mathrm{d}\xi+k_{\mathrm{ca},y}\int_0^{l_s}N_{Y,sb}^{\mathrm{T}}N_{Y,sb}\mathrm{d}\xi\right] \tag{24}$$

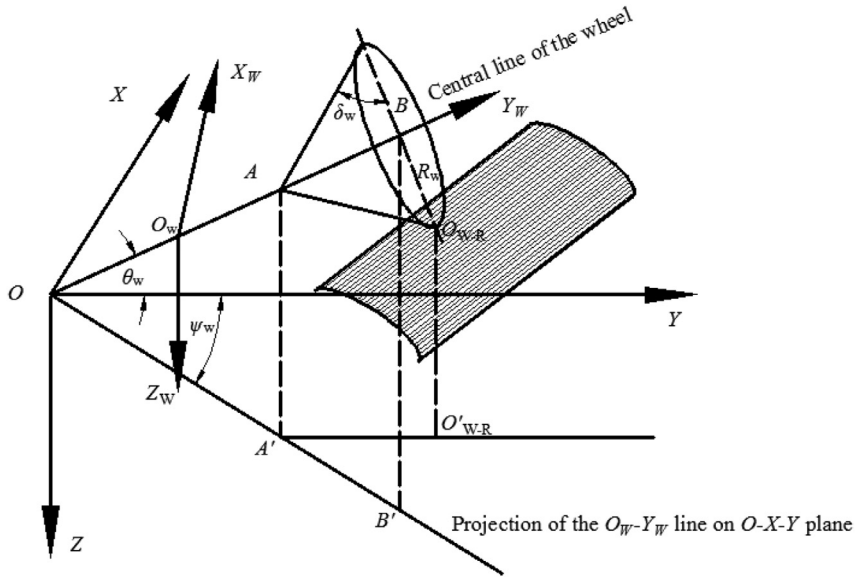

Fig. 2. Wheel-rail coupled model [24].

with

$$N_{Z,sb} = N_{Zs} - N_{Zb}, \quad N_{Zb} = \left[N_{Zr} \left(B_r - \frac{b_s}{2} + \zeta \right) N_{\theta_X r} \right],$$
$$N_{Y,sb} = N_{Ys} - N_{Yb}, \quad N_{Yb} = \begin{bmatrix} N_{Yr} & H_r & N_{\theta_X r} \end{bmatrix},$$

The damping matrix, $\tilde{\boldsymbol{C}}_{s-b}$, has almost the same expression as $\tilde{\boldsymbol{K}}_{s-b}$ just by substituting the stiffness coefficients "$k_{ca,z}$" and "$k_{ca,y}$" with damping coefficients "$c_{ca,z}$" and "$c_{ca,y}$" .

In the same manner as Eq. (23), the matrices of stiffness and damping should be partitioned as

$$\begin{bmatrix} \bar{\boldsymbol{K}}_{ss,2} & \boldsymbol{K}_{sb} \\ \boldsymbol{K}_{bs} & \bar{\boldsymbol{K}}_{bb,1} \end{bmatrix} = \tilde{\boldsymbol{K}}_{s-b}; \begin{bmatrix} \bar{\boldsymbol{C}}_{ss,2} & \boldsymbol{C}_{sb} \\ \boldsymbol{C}_{bs} & \bar{\boldsymbol{C}}_{bb,1} \end{bmatrix} = \tilde{\boldsymbol{C}}_{s-b}, \tag{25}$$

Thus the stiffness and damping matrix of the slab will be replaced by $\boldsymbol{K}_{ss}+\bar{\boldsymbol{K}}_{ss,1}+\bar{\boldsymbol{K}}_{ss,2}$ and $\boldsymbol{C}_{ss}+\bar{\boldsymbol{C}}_{ss,1}+\bar{\boldsymbol{C}}_{ss,2}$.

2.2.10. Sub-matrices for the Girder–Pier interactions

The matrices for girder-pier interactions are marked with the subscripts "*bp*" and "*pb*", which are derived by the interactions between the girder and the pier connected by the cement asphalt mortar (CAM).

The stiffness matrix, $\tilde{\boldsymbol{K}}_{b-p}$, with order of $(N_b \times n_b + N_p \times n_p) \times (N_b \times n_b + N_p \times n_p)$, can be written as

$$\tilde{\boldsymbol{K}}_{b-p} = \sum_{h=1}^{N_p} \left[k_{p,z} N_{Z,bp}^{T} N_{Z,bp} + k_{p,y} N_{Y,bp}^{T} N_{Y,bp} \right] \tag{26}$$

with $N_{Z,bp} = N_{Zs} - N_{Zp}$, $N_{Zb} = 1$; $N_{Y,bp} = N_{Yb} - N_{Yp}$, $N_{Yp} = 1$;

The damping matrix, $\tilde{\boldsymbol{C}}_{b-p}$, can be obtained by replacing the stiffness coefficients "$k_{p,z}$" and "$k_{p,y}$" in the corresponding stiffness matrix with damping coefficients "$c_{p,z}$" and "$c_{p,y}$" .

The matrices of stiffness and damping should be partitioned as

$$\begin{bmatrix} \bar{\boldsymbol{K}}_{bb,2} & \boldsymbol{K}_{bp} \\ \boldsymbol{K}_{pb} & \bar{\boldsymbol{K}}_{pp,1} \end{bmatrix} = \tilde{\boldsymbol{K}}_{b-p}; \begin{bmatrix} \bar{\boldsymbol{C}}_{bb,2} & \boldsymbol{C}_{bp} \\ \boldsymbol{C}_{pb} & \bar{\boldsymbol{C}}_{pp,1} \end{bmatrix} = \tilde{\boldsymbol{C}}_{b-p}, \tag{27}$$

Accordingly, the stiffness and damping matrix of the girder will be assembled as $\boldsymbol{K}_{bb}+\bar{\boldsymbol{K}}_{bb,1}+\bar{\boldsymbol{K}}_{bb,2}$ and $\boldsymbol{C}_{bb}+\bar{\boldsymbol{C}}_{bb,1}+\bar{\boldsymbol{C}}_{bb,2}$, and the stiffness and damping matrix of the pier will be obtained by $\boldsymbol{K}_{pp}+\bar{\boldsymbol{K}}_{pp,1}$ and $\boldsymbol{C}_{pp}+\bar{\boldsymbol{C}}_{pp,1}$.

2.2.11. Load vectors

The wheel-rail contact geometries are almost the most important and complex part in the whole train-track-bridge dynamic model. In the wheel-rail coupled model [30], the yaw, pitch, roll, transverse and bounce motions of the wheelset and the transverse, bounce and torsional motions of the rail are considered with a comprehensive way, as shown in Fig. 2, the wheel-rail contacts will therefore be treated as a three-dimensional (3-D) nonlinear and asymmetry problem inevitably.

The dynamic load acting on the wheelset is derived by the work of the force/moment on transverse, bounce, roll, yaw and pitch motions of the wheelset respectively, that is [24],

$$\boldsymbol{F}_{\mathrm{w}} = \sum_{j=1}^{2+N_v}\sum_{i=1}^{4}\boldsymbol{F}_{\mathrm{w},i} \tag{28}$$

with

$$\boldsymbol{F}_{\mathrm{w},i} = \begin{bmatrix} F_{\mathrm{w},Yi} \\ F_{\mathrm{w},Zi} \\ F_{\mathrm{w},\phi i} \\ F_{\mathrm{w},\psi i} \\ F_{\mathrm{w},\beta i} \end{bmatrix} = \begin{bmatrix} F_{Yli}+F_{Yri}+M_w\bar{g}\varphi_i - M_wV^2/R_i - M_w\mathrm{r}_0\ddot{\varphi}_{wi} \\ F_{Zli}+F_{Zri}+M_w\bar{g}+M_wa_0\ddot{\varphi}_{wi}+M_wV^2/R_i\varphi_{wi} \\ a_0(F_{Zri}-F_{Zli})-r_{li}F_{Yli}-r_{ri}F_{Yri}+I_{wY}(\dot{\beta}_{wi}-\Omega)(\dot{\psi}_{wi}+V/R_i)-I_{wX}\ddot{\varphi}_{wi} \\ a_0(F_{Xli}-F_{Xri})-a_0\psi_{wi}(F_{Yli}-F_{Yri})+M_{Zli}+M_{Zri}+I_{wY}(\dot{\beta}_{wi}-\Omega)(\dot{\phi}_{wi}+\dot{\varphi}_{wi})-I_{wZ}V\dot{\lambda}_{wi} \\ r_{li}F_{Xli}+r_{ri}F_{Xri}+\psi_{wi}(r_{li}F_{Yli}+r_{ri}F_{Yri})+M_{Yli}+M_{Yri} \end{bmatrix},$$

where the subscript "i", i=1, 2, 3, 4, denotes the ith wheelset; F_{Xli} and F_{Xri} denote the longitudinal forces acting on the left- and right- side of wheel/rail contact interface, respectively; F_{Yli} and F_{Yri} denote the transverse forces acting on the left- and right- side of wheel/rail contact interface, respectively; F_{Zli} and F_{Zri} denote the vertical forces acting on the left- and right-side of the wheel/rail contact interface, respectively; M_{Zli} and M_{Zri} are the moment of force around Z-axis, respectively; M_{Yli} and M_{Yri} are the moment of force around Y-axis, respectively; $\dot{\beta}_{wi}$, $\dot{\psi}_{wi}$ and $\dot{\phi}_{wi}$ denote the pitch, yaw and rolling velocity of the ith wheelset; ψ_{wi} is the yaw angle.

The forces acting on the centroid of mass of the car body are mainly derived from the work of force/moment at motions of transverse, bounce, rolling and yaw when the vehicle passes through the curved tracks, namely

$$\boldsymbol{F}_{\mathrm{c}} = \sum_{i=1}^{2+N_v}\boldsymbol{F}_{\mathrm{c},i} \tag{29}$$

with

$$\boldsymbol{F}_{\mathrm{c},i} = \begin{bmatrix} F_{\mathrm{c},Yi} \\ F_{\mathrm{c},Zi} \\ F_{\mathrm{c},\phi i} \\ F_{\mathrm{c},\psi i} \end{bmatrix} = \begin{bmatrix} M_cg\varphi_c - M_cV^2/R_c - M_c(\mathrm{r}_0+H_{\mathrm{tw}}+H_{\mathrm{bt}}+H_{\mathrm{cb}})\ddot{\varphi}_c \\ M_cg+M_cV^2/R_c\varphi_c+M_ca_0\ddot{\varphi}_c \\ -I_{cX}\ddot{\varphi}_c \\ -I_{cZ}V\dot{\varsigma}_c \end{bmatrix},$$

The forces acting on the centroid of mass of the bogie frames are mainly derived from the work of force/moment at motions of transverse, bounce, rolling and yaw when the vehicle passes through the curved tracks, namely

$$\boldsymbol{F}_{\mathrm{b}} = \sum_{i=1}^{2+N_v}\sum_{k=1}^{2}\boldsymbol{F}_{k} \tag{30}$$

with

$$\begin{bmatrix} F_{k,Y} \\ F_{k,Z} \\ F_{k,\phi} \\ F_{k,\psi} \end{bmatrix} = \begin{bmatrix} M_kg\varphi_k - M_kV^2/R_k - M_k(\mathrm{r}_0+H_{\mathrm{tw}})\ddot{\varphi}_k \\ M_kg+M_kV^2/R_k\varphi_k+M_ka_0\ddot{\varphi}_k \\ -I_{kX}\ddot{\varphi}_k \\ -I_{kZ}V\dot{\varsigma}_k \end{bmatrix},$$

where k=1 and 2 represent the front bogie frame, "Gq", and rear bogie frame, "Gh", respectively.

With regard to the track systems, rail is the component that directly bears the dynamic loads from the train, and the dynamic force acting on the transverse, vertical and torsional displacement can be expressed as

$$\boldsymbol{F}_{r} = \sum_{i=1}^{2+N_v}\sum_{j=1}^{4}\sum_{l=1}^{2}\boldsymbol{F}_{k,l,j} \tag{31}$$

with

$$\boldsymbol{F}_{k,l,j} = \begin{bmatrix} F_{Y,lj} \\ F_{Z,lj} \\ M_{T,lj} \end{bmatrix} = \begin{bmatrix} F_{Yl}\boldsymbol{N}_{\mathrm{Yr},j} \\ F_{Zl}\boldsymbol{N}_{\mathrm{Zr},j} \\ (F_{Zl}l_{hi}+F_{Yl}l_{vi})\boldsymbol{N}_{\theta_{\mathrm{X}}\mathrm{T},j} \end{bmatrix},$$

where the subscript "l" denotes the left or right side of the rail; the subscript "j" denotes the jth wheel-rail contact pair; $F_{Y,lj}$, $F_{Z,lj}$ and $M_{T,lj}$ denote the equivalent lateral, vertical and torsional forces acting on the centroid of the rail.

According to above presentations, one can obtained that $\boldsymbol{F}_t=\boldsymbol{F}_{\mathrm{c}}+\boldsymbol{F}_{\mathrm{b}}+\boldsymbol{F}_{\mathrm{w}}$, $\boldsymbol{F}_s$=0, $\boldsymbol{F}_b$=0, $\boldsymbol{F}_p$=0.

Till now, the dynamic sub-matrices and loading vectors in Eq. (1) have been fully revealed to effectively couple the train, track and bridge systems as an entire system. By adopting numerical integration methods, the system responses of train, track and bridge can be obtained simultaneously.

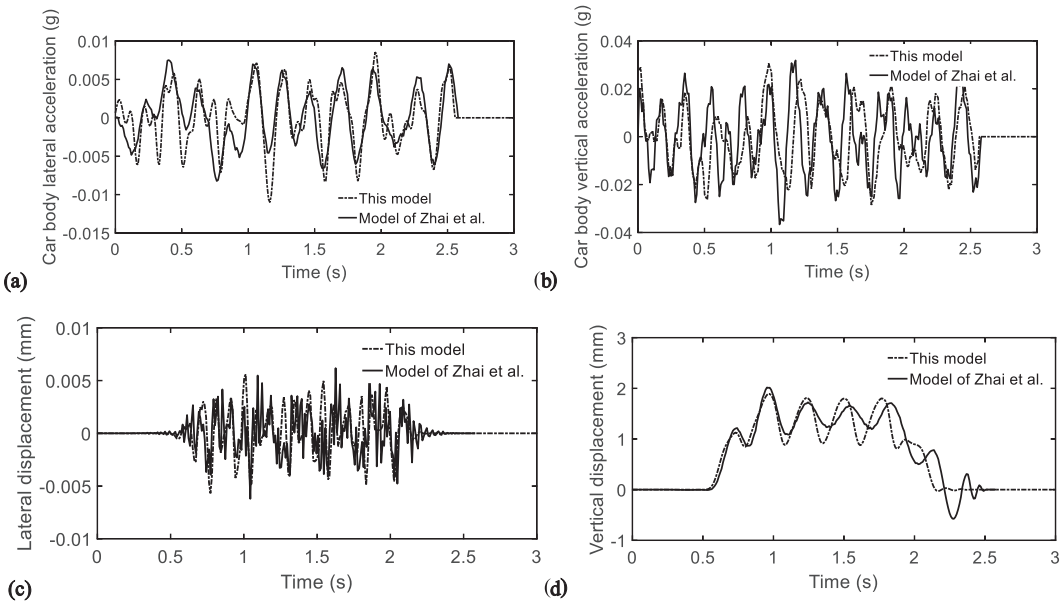

Fig. 3. Comparisons with the model of Zhai et al. [1] on car body accelerations and the vibrations at the mid-span of the bridge (a. lateral acceleration of the car body; b. vertical acceleration of the car body; c. lateral displacement of the girder at the mid-span; d. vertical displacement of the girder at the mid-span).

2.2.12. Comparison with general solutions

For validating the practicality of this dynamical model compiled in a computer program, a comparison to a three-dimensional model by Zhai et al. [10] is conducted. It is assumed that an entire train grouped by five vehicles runs on the bridge (five-span simply supported beam-bridge) with a constant velocity (300 km/h).

Fig. 3 presents the comparisons on the dynamic responses of the bridge at the second mid-span and car body accelerations, from which one can observe that the dynamic results respectively derived from these two models coincide relatively well with each other. The accurateness and practicality of this model is therefore illustrated clearly. However it should be noted that there inevitably exist slight deviations between the results because of the completely different methods in the model constructions, see for example: the coupler and draft system between the car bodies of vehicles ignored in [10] are considered effectively in this model; in this model, the track and the bridge have been united an entire system, while they are solved separately in [10].

3. Characterization of the temporal-spatial stochasticity for the coupled system

The model constructed in Section 2 is developed to characterize the train-track-bridge interactions with respect to deterministic system parameters and excitations, e.g., track random irregularities. It has been pointed out previously that the train-track-bridge systems are essentially random in nature, especially the track-bridge system, which holds significantly inhomogeneous characteristics in the spatial domain, moreover, the random field of dynamic parameters is constantly evolved corresponding to the cyclic train-track-bridge interactions.

3.1. Joint simulation based on Monte-Carlo Method (MCM) and Karhunen-Loève Expansion (KLE)

3.1.1. Random field representation

By neglecting the stochasticity of the system components in Y direction, the random variables of track-bridge systems can be expressed as $\boldsymbol{\Omega}(x, z, t)$, where x represents the longitudinal abscissa of the tracks, z represents the vertical coordinate and t represents the time process. Thus the unified field of system structures can be expressed by

$$\boldsymbol{T}_{\Theta} = \boldsymbol{T}(\boldsymbol{\Omega}(x, z, t)),\ \boldsymbol{\Omega} \in R^3 \tag{32}$$

where R^3 represents the three-dimensional Euclidean space, Θ represents the definition domain of the random field, and the variable z is mainly applied to express the vertically layered characteristics of track and bridge structures, namely different physical and mechanical parameters of structures.

With respect to the determined structural parameters z_{υ}, $\upsilon = 1, 2, ..., M$ and the time point t_k, k=1, 2, ..., N, the spatial distribution of $\boldsymbol{\Omega}(x, z, t)$, which is regarded to follow a certain type of probability distribution, can be characterized by

$$\boldsymbol{T}(\boldsymbol{\Omega}(x, z_{\upsilon}, t_{\kappa})) \sim \boldsymbol{P}(\tilde{V}) \tag{33}$$

where $\boldsymbol{P}(\bullet)$ represents the possible probability distribution type, and $\tilde{V}$ represents the corresponding characteristic parameters, e.g., the statistical mean and standard deviation of normal distribution, the degree of chi square distribution, etc.

Generally, the longitudinal coordinate of the rail line represented by parameter x will be with a huge magnitude once considering the whole bridge sections existing in a railway line. Therefore, a longitudinal division towards the random space is conducted by considering the limit length of numerical calculations, namely

$$x = \cap x_l,\ x_l \in (0, S^{tot}/N] \tag{34}$$

where S^{tot} represents the total railway length, N represents the number of division, and $l = 1, 2, ..., N$.

In summary, the random field of track-bridge systems can be further transformed from Eq. (32) as

$$\boldsymbol{T}_\Theta = \boldsymbol{T}(\boldsymbol{\Omega}(x_l, z_\upsilon, t_\kappa)) \tag{35}$$

3.1.2. Monte-Carlo simulation

In numerical studies, the random field represented by Eq. (35) is conventionally modelled by MCM that is perhaps the most robust approach in random analysis. For a certain time point t_κ, the space vector in Eq. (35) can be expounded as a two-dimensional matrix form

$$\boldsymbol{T}_\Theta = \begin{pmatrix} \boldsymbol{T}(u(x_1, z_1, t_\kappa)) & \boldsymbol{T}(u(x_2, z_1, t_\kappa)) & \cdots & \boldsymbol{T}(u(x_N, z_1, t_\kappa)) \\ \vdots & \vdots & \ddots & \vdots \\ \boldsymbol{T}(u(x_1, z_{1\times H}, t_\kappa)) & \boldsymbol{T}(u(x_2, z_{1\times H}, t_\kappa)) & \cdots & \boldsymbol{T}(u(x_N, z_{1\times H}, t_\kappa)) \\ \vdots & \vdots & \ddots & \vdots \\ \boldsymbol{T}(u(x_1, z_{M\times H}, t_\kappa)) & \boldsymbol{T}(u(x_2, z_{M\times H}, t_\kappa)) & \cdots & \boldsymbol{T}(u(x_N, z_{M\times H}, t_\kappa)) \end{pmatrix}_{(M\times H)\times N} \tag{36}$$

where the subscript "H" denotes the number for a specific variable in one sample.

To the actual random variables z_υ, which are assumed to follow an already known probability density function (PDF) $f_Z(z_\upsilon)$, the cumulative distribution function (CDF), a monotonic function, can be derived by

$$F_Z(z_\upsilon) = \int_{-\infty}^{z_\upsilon} f_Z(z_\upsilon)\mathrm{d}z_\upsilon,\ \upsilon = 1, 2, ..., M, \tag{37}$$

The correlation matrix between z_υ can be expressed by

$$R_{M\times M} = \begin{pmatrix} 1 & r_{12} & \dots & r_{1M} \\ r_{21} & 1 & \dots & r_{2M} \\ \vdots & \vdots & \dots & \vdots \\ r_{M1} & r_{M2} & \dots & 1 \end{pmatrix} \tag{38}$$

For obtaining random series of z_υ that satisfies Eqs. (37) and (38), based on a linear-nonlinear transformation method [31], the steps for achieving this goal can be followed by

(1) Let g_υ be the variable following Gaussian distribution, that is,

$$f_G(g_\upsilon) = \frac{1}{\sqrt{2\pi}\,\sigma_{g_\upsilon}} \exp\left(-\frac{(z-\mu_{g_\upsilon})^2}{2\sigma_{g_\upsilon}^2}\right) \tag{39}$$

where μ_{g_υ} and σ_{g_υ} respectively represent the statistical average and standard deviation with respect to the variable g_υ. For simplifying the transformation, it is practical to set $\mu_{g_\upsilon} = 0$ and $\sigma_{g_\upsilon} = 1$.

In the same manner as Eq. (37), the CDF of g_υ can be obtained by

$$F_G(g_\upsilon) = \int_{-\infty}^{g_i} f_G(g_\upsilon)\mathrm{d}g_\upsilon \tag{40}$$

Based on Eqs. (37) and (40), the nonlinear transformation between x_υ and g_υ can be estimated as

$$x_\upsilon = \hbar_\upsilon(g_\upsilon) = F_Z^{-1}(F_G(g_\upsilon)) \tag{41}$$

where $\hbar(\bullet)$ denotes the nonlinear transformation operator for argument $(\bullet)$; $F^{-1}(\bullet)$ denotes the inverse function.

(2) Deriving the correlation coefficient $r_{g_ig_j}$ through $r_{x_ix_j}$, $i, j = 1, 2, ..., M$, $i \neq j$, that is [30,31],

$$\begin{aligned} r_{x_ix_j} &= \frac{E\left[(x_i - \mu_{x_i})(x_j - \mu_{x_j})\right]}{\sigma_{x_i}\sigma_{x_j}} \\ &= \int_{-\infty}^{\infty}\int_{-\infty}^{\infty} \frac{(\ell_i(g_i) - \mu_{x_i})}{\sigma_{x_i}} \frac{(\ell_j(g_j) - \mu_{x_j})}{\sigma_{x_j}} f_{GG}(g_i, g_j)\mathrm{d}g_i\mathrm{d}g_j \end{aligned} \tag{42}$$

with

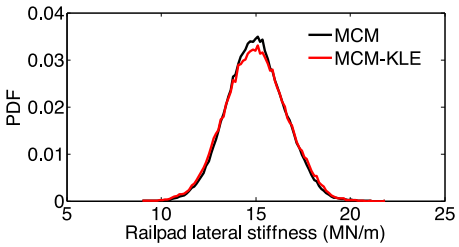

Fig. 4. PDF comparison between the results of MCM and MCM-KLE.

$$f_{GG}(g_i, g_j) = \frac{1}{2\pi\sqrt{1-r_{g_ig_j}^2}} \exp\left[-\frac{(g_i^2 - 2r_{g_ig_j}g_ig_j + g_j^2)}{2(1-r_{g_ig_j}^2)}\right];\ \mu_x = E(x);\ \sigma_x = E(x^2) - [E(x)]^2,$$

in Eq. (42), E denotes the mathematical expectation, and the relationship between $r_{g_ig_j}$ and $r_{x_ix_j}$ has been connected definitely. For solving the integration of Eq. (42), Newton–Raphson iteration method is applied [32], and then, the correlation matrix $\tilde{R}_{M\times M}$ with regard to g_i can be confirmed accordingly.

(3) Using Monte-Carlo method, the random vector of g_i can be assembled as

$$(\boldsymbol{G} = (\boldsymbol{G}_1, G_2, ..., G_M)_{L\times M}) \tag{43}$$

And then, the Cholesky decomposition is conducted on $\tilde{R}_{M\times M}$, and the $\mathbf{G}$ will be updated by

$$\boldsymbol{G}' = \boldsymbol{G}_{L\times M}C_{r,M\times M} \tag{44}$$

with $\tilde{R}_{M\times M} = C_g^{\mathrm{T}}C_g$, the updated random vector $\boldsymbol{G}'$ will satisfy the correlation matrix $\tilde{R}_{M\times M}$.

(4) Finally, through the nonlinear transformation, the standardized random vector $\boldsymbol{G}'$ can be transformed into arbitrary correlated pseudorandom variables, namely the space vector of the random filed by

$$\boldsymbol{T}_\Theta = \hbar(\boldsymbol{G}') \tag{45}$$

3.1.3. Dimension reduction based on Karhunen–Loève Expansion (KLE)

MCM is generally accompanied by rather low computational efficiency and convergence in the random analysis. In the current work, Karhunen–Loève Expansion (KLE) is further applied to achieve a dimensional reduction for the random filed of track-bridge systems.

Based on the definition of KLE [33], the random field of track structures can be further expressed by

$$\boldsymbol{T}_\Theta \approx E[\boldsymbol{T}_\Theta] + \sum_{i=1}^{N_s}\sqrt{\lambda_i}\boldsymbol{u}_i\zeta_i \tag{46}$$

with $\mathrm{E}[\zeta_i\zeta_j] = \delta_{ij}$, where δ_{ij} is the Kronecker delta, $\mathrm{E}[\cdot]$ denotes the expectation operation; $E[\boldsymbol{T}_\Theta]$ is the mean of the stochastic process, ζ_i are orthonormal random variables.

The set of deterministic functions λ_i and $\boldsymbol{u}_i$ are eigenvalues and eigenvectors, respectively, with satisfying the following equation, namely

$$\boldsymbol{C}_{XX}\boldsymbol{\mu} = \lambda\boldsymbol{\mu} \tag{47}$$

where $\boldsymbol{C}_{XX}$ represents an bounded, symmetric and positive definite auto-covariance function of $\boldsymbol{T}_\Omega$. The projection basis $\{\boldsymbol{\mu}_1, \boldsymbol{\mu}_2, ..., \boldsymbol{\mu}_{N_s}\}$ is chosen orthonormal in the sense that, for all γ and ℓ:

$$(\boldsymbol{\mu}^\gamma)^T\boldsymbol{\mu}^\ell = \delta_{\gamma\ell} \tag{48}$$

The KLE is capable of capturing the spatial correlation of the fields, guaranteeing the randomicity of signals and greatly reducing the calculation samples by $N_s \ll N$.

For more details about KLE, Refs. [34,35] can be consulted for references.

For validating the effectiveness of the MCM-KLE method, Fig. 4 plots a PDF comparison between the random samples respectively simulated by MCM and MCM-KLE with regard to the random variable, i.e., lateral stiffness of fastener. As seen from Fig. 4, the statistical properties for the simulating results of these two method coincide well with each other, however, there are 2000 samples in the MCM, but by applying MCM-KLE, the sampling number is reduced to 174, thus the united MCM-KLE method greatly increases the computational efficiency.

3.2. Track irregularity probabilistic model

Xu and Zhai [36] proposed a track irregularity probabilistic model (TIPM) to select representative and realistic track irregularity sets for a high-efficient characterization of the statistical properties of track geometries.

The abbreviated procedures are illustrated as

1) Divide the measured track irregularities $\boldsymbol{I}(s)$ into N segments, namely

$$\boldsymbol{I}(s) = \cup(\boldsymbol{I}(\tilde{s}_k)) \tag{49}$$

where s denotes the distance along the track, $k = 1, 2, ..., N$, $\tilde{s}_k \in (S_{tot}(k-1)/N, S_{tot}k/N]$,

2) Set $\ell(\bullet)$ as the power spectral density (PSD) operator, and the PSD of $\boldsymbol{I}(\tilde{s}_k)$ can be obtained by $P_k(\omega) = \ell(\boldsymbol{I}(\tilde{s}_k))$;
3) With a series of derivations, the probability density function (PDF) of $P_k(\omega)$ denoted by $\Gamma(P_k(\omega))$ can be derived.
4) Based on time-frequency transformation approach [35], the equivalent time domain track irregularities $\tilde{\boldsymbol{I}}(\tilde{s}_k)$ used as the exciting inputs of the interaction model can be performed on $P(k)$, and assuming $\Gamma(P_k(\omega)) = \Gamma(\tilde{\boldsymbol{I}}(\tilde{s}_k))$.
5) With cognition of the probability distribution of $P_k(\omega)$, it is rather convenient to select representative PSD function, i.e., $P_r(\omega)$, in which r is the selected sample of PSD, $r = 1, 2, ..., \tilde{N}$, using random simulation methods. Generally, it is obvious that $\tilde{N} \ll N$, while the statistical properties of $\boldsymbol{I}(s)$ in amplitudes and frequencies are defined without information loss, and being contained in $P_r(\omega)$.

3.3. Temporal evolution of system dynamic characteristics

As to the evolution of system parameters, the experimental studies in situ or lab have rarely been reported yet, thus the formulaic expressions used to program the variation of parameters against time cannot be revealed in the present study, and accordingly, the coefficients of variation (COV) are simply adopted to characterize the evolution of random system parameters, as shown in Ref. [26].

To the track irregularities, track maintenance department will periodically detect the rail profile deformations using track inspection car. The track irregularity probabilistic model mentioned in last part is developed to extract the realistic and representative samples from the massive track irregularity data, based on which the strategy on statistically characterizing the temporal evolution of track random irregularities can be further achieved by equivalently transforming the amplitude evolution of track irregularities into its power spectral density evolution, the detailed procedures can be followed as below

1) The power spectrums of track irregularities at time t_i and t_{i+1} denoted by $\boldsymbol{P}_{\varsigma,t_i}(\omega)$ and $\boldsymbol{P}_{\varsigma,t_{i+1}}(\omega)$ respectively, where the subscript "ζ" denotes the track irregularity type, are summarily obtained by the spectral estimation method, indicating that the amplitude-frequency properties of $\boldsymbol{I}_{\varsigma,t_i}(s)$ will be evolved from $\boldsymbol{P}_{\varsigma,t_i}(\omega)$ to $\boldsymbol{P}_{\varsigma,t_{i+1}}(\omega)$ during the time period of $(t_i, t_{i+1}]$, thus the spectral evolution can be figured out by

$$\tilde{\boldsymbol{P}}_{\varsigma,(t_i,t_{i+1}]}(\omega) = \boldsymbol{P}_{\varsigma,t_{i+1}}(\omega) - \boldsymbol{P}_{\varsigma,t_i}(\omega) \tag{50}$$

2) For the analytical convenience, a spectral density matrix with order of $E \times W$ can be assembled by

$$\boldsymbol{\Omega}_{\varsigma,i}(q,\omega) = \left[\cup \boldsymbol{P}_{\varsigma,t_i,q}(\omega_d)\right]_{E\times W},\ q = 1, 2, ..., E, \tag{51}$$

where the subscript "i" and "q" denotes the time interval of measurement $(t_i, t_{i+1}]$ and the qth track irregularity power spectrum with respect to the qth track portion, E is the total number of power spectrums and the subscript "W" denotes the total number of frequency points. In the same manner, a spectral density evolution matrix $\tilde{\boldsymbol{\Omega}}_{\varsigma,i}(q,\omega)$ can be obtained by $[\boldsymbol{\Omega}_{\varsigma,i+1}(q,\omega) - \boldsymbol{\Omega}_{\varsigma,i}(q,\omega)]$.

3) Obviously, with large-scale and long-term measurements, namely i=1, 2, ..., T, T is a relatively large value, a completely mapping relation between $\boldsymbol{\Omega}_{\varsigma,i}(q,\omega)$ and $\tilde{\boldsymbol{\Omega}}_{\varsigma,i}(q,\omega)$ can be numerically matched, where $\boldsymbol{\Omega}_{\varsigma}(q,\omega) = \cup \boldsymbol{\Omega}_{\varsigma,i}(q,\omega)$ and $\tilde{\boldsymbol{\Omega}}_{\varsigma}(q,\omega) = \cup \tilde{\boldsymbol{\Omega}}_{\varsigma,i}(q,\omega)$.
4) Let $\boldsymbol{P}_{\varsigma,l}(\omega_d) = \min[\tilde{\boldsymbol{\Omega}}_{\varsigma}(q,\omega_d)]$ and $\boldsymbol{P}_{\varsigma,u}(\omega_d) = \max[\boldsymbol{\Omega}_{\varsigma}(q,\omega_d)]$, where $\min[\bullet]$ and $\max[\bullet]$ denote the minimum and maximum operators respectively. Because the spectral densities are discretely distributed, the amplitude domain of $\boldsymbol{P}_{\varsigma}(\omega_d)$ can be divided into

$$\boldsymbol{P}_{\boldsymbol{\Theta}_{\varsigma,g}}(\omega_d) \in [\boldsymbol{P}_{\varsigma,l}(\omega_d) + g\tilde{\boldsymbol{P}}(\omega_d), \boldsymbol{P}_{\varsigma,l}(\omega_d) + (g+1)\tilde{\boldsymbol{P}}(\omega_d)] \tag{52}$$

with $\tilde{\boldsymbol{P}}(\omega_d) = \mathrm{int}[\frac{\boldsymbol{P}_{\varsigma,u}(\omega_d) - \boldsymbol{P}_{\varsigma,l}(\omega_d)}{Z}]$, $0 \le g \le Z$-1,

where $\tilde{\boldsymbol{P}}$ is the discrete interval of spectral densities; Z is the total partition number; $\mathrm{int}[\cdot]$ is an operator used to obtain the largest integer being smaller than the number in the bracket; the subscript " $\boldsymbol{\Theta}_{\varsigma,g}$" denotes the field of spectral densities satisfying Eq. (52).

5) It is certain that the spectral densities $\boldsymbol{P}_{\boldsymbol{\Theta}_{\varsigma,g}}(\omega_d)$ included in the field of $\boldsymbol{\Theta}_{\varsigma,g}$ will correspond to different evolution values, $\tilde{\boldsymbol{P}}_{\boldsymbol{\Theta}_{\varsigma,g}}(\omega_d) \in \tilde{\boldsymbol{\Omega}}_{\varsigma}(\omega_d)$. Based on probabilistic statistics, the probability density function (PDF) of the evolutions denoted by $f_{\varsigma,\omega_d}(\tilde{\boldsymbol{P}}_{\boldsymbol{\Theta}_{\varsigma,g}})$ can be determined by $\tilde{\boldsymbol{P}}_{\boldsymbol{\Theta}_{\varsigma,g}}(\omega_d)$.
6) It is regarded that the evolution of the spectral densities within $\boldsymbol{\Theta}_{\varsigma,g}$ will follow the same PDF characteristics. Therefore, a cumulative probability index $p_{\varsigma} \in (0, 1)$ is introduced to uniquely confirm the evolution value of spectral density over $\boldsymbol{P}_{\varsigma,t_i}(\omega)$, namely

$$\tilde{\boldsymbol{P}}'_{t_i}(\omega; p_{\varsigma}) = F^{-1}_{\varsigma,\omega_d}(p_{\varsigma}) \tag{53}$$

with $F_{\varsigma,\omega_d}(\tilde{\boldsymbol{P}}_{\varsigma,g}) = \int_{-\infty}^{\tilde{\boldsymbol{P}}_{\varsigma,g}} f_{\varsigma,\omega_d}(\tilde{\boldsymbol{P}}_{\boldsymbol{\Theta}_{\varsigma,g}})\mathrm{d}\tilde{\boldsymbol{P}}_{\varsigma,g}$,

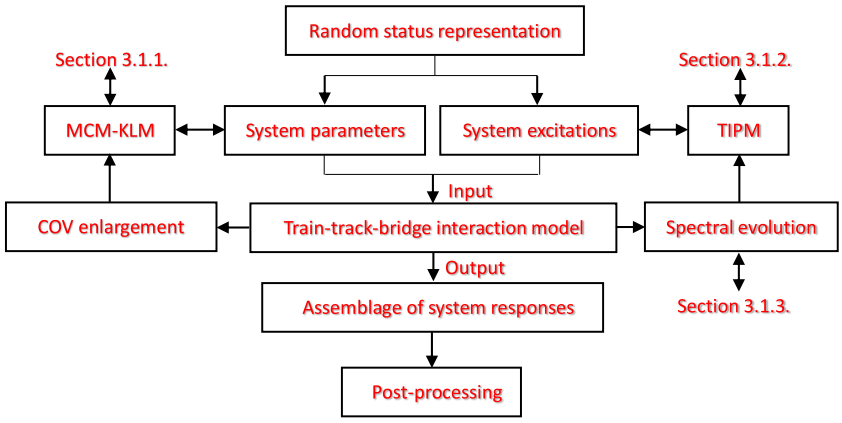

Fig. 5. Modelling framework for train-track-bridge stochastic model.

where $F_{\varsigma,\omega_d}(\cdot)$ is the CDF of $f_{\varsigma,\omega_d}(\cdot)$.

7) On the basis of Eq. (53), the evolution spectrum $\boldsymbol{P}'_{t_{i+1}}(\omega; p_\varsigma)$ can be obtained by

$$\boldsymbol{P}'_{t_{i+1}}(\omega; p_\varsigma) = \boldsymbol{P}_{\varsigma,t_i}(\omega) + \tilde{\boldsymbol{P}}'_{t_i}(\omega; p_\varsigma) \tag{54}$$

8) It should be noted that $\boldsymbol{P}'_{t_{i+1}}(\omega; p_\varsigma)$, which is determined by the probability index p_ς and evolution domain $\tilde{\boldsymbol{P}}_{\boldsymbol{\Theta}_{\varsigma,g}}(\omega_d)$, is an uncertain quantity, thus it can be selected by random simulation methods.

By implementing the time-frequency transformation process [36], the evolution spectrum $\boldsymbol{P}'_{t_{i+1}}(\omega; p_\varsigma)$ in Eq. (54) can be equivalently transformed into time-domain track irregularities $\boldsymbol{I}'_{t_{i+1}}(s)$. By loading $\boldsymbol{I}'_{t_{i+1}}(s)$ into the dynamic model, the dynamic performance of train-track-bridge systems can be assessed in light of different evolutionary status of excitations.

4. Construction of the temporal-spatial stochastic model

Till now, the work related to the establishment of the dynamic model, random simulation and characterization of the system parameters and excitations in temporal-spatial domain have all been accomplished properly. The essence for constructing the train-track-bridge temporal-spatial stochastic model lays on uniting the random physical-mechanical status of the systems and the dynamical interaction mechanisms.

Summarily, the modelling framework can be illustrated as Fig. 5

5. Case studies

In the numerical studies, it is assumed that there are two motor cars in the front and rear part of the train, and with three trailer cars contained in the middle, the related parameters have been presented in Ref. [18]; besides, a five span simple support beam bridge is constructed by 32-meter beam elements, the related dynamic parameters of the bridge are listed in Ref. [18].

5.1. Case 1: characteristics of system responses for train-track-bridge interactions

Rather different from common infrastructural systems, the railway bridges normally assumed as beam elements offer more flexible supports to the train-track systems in general, thus the dynamic response of train-track-bridge systems might possess unique characteristics.

Fig. 6 plots the time-varying rail displacements by tracking the wheel-rail contact points. It can be seen from Fig. 7 that the time processes of rail displacements show significantly non-stationary and asymmetry characteristics; when the wheelsets arrive at the mid-span of the bridge, the vertical dynamic deflections D_{zr} of the track-bridge structures reach the maximum responses; as to the rail lateral displacement D_{yr}, though, without that significantly asymmetry feature as D_{zr}, we can still observe that the D_{yr} has obviously deviated from the normal central line.

Moreover, Fig. 7 illustrates the representative responses of the displacement and the acceleration with specific to the point at the mid-span of the bridge girder, from which one can observe that when the first motor car approaches to the specific point, the vertical deflection will be gradually increased to reach the first peak with loading of a half weight of a car, and then the deflection will reach the maximum after a full weight of the car acting on the girder of the bridge, when the train gradually passes through the mid-span, the deflection of the bridge structures will accordingly decay to original

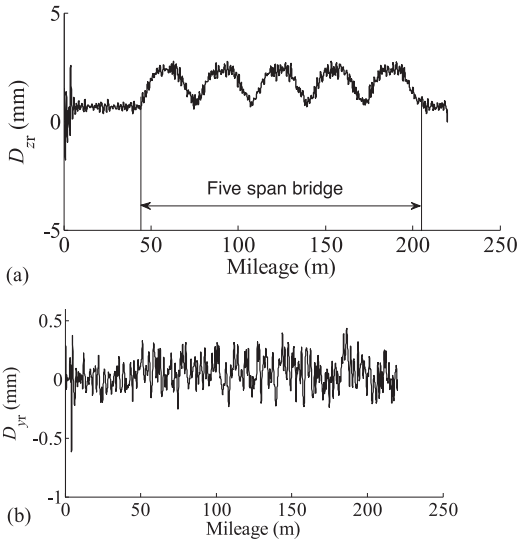

Fig. 6. The time-varying displacement of the rail following the trail of the 1st wheelset of the trailer car (a. vertical displacement; b. lateral displacement).

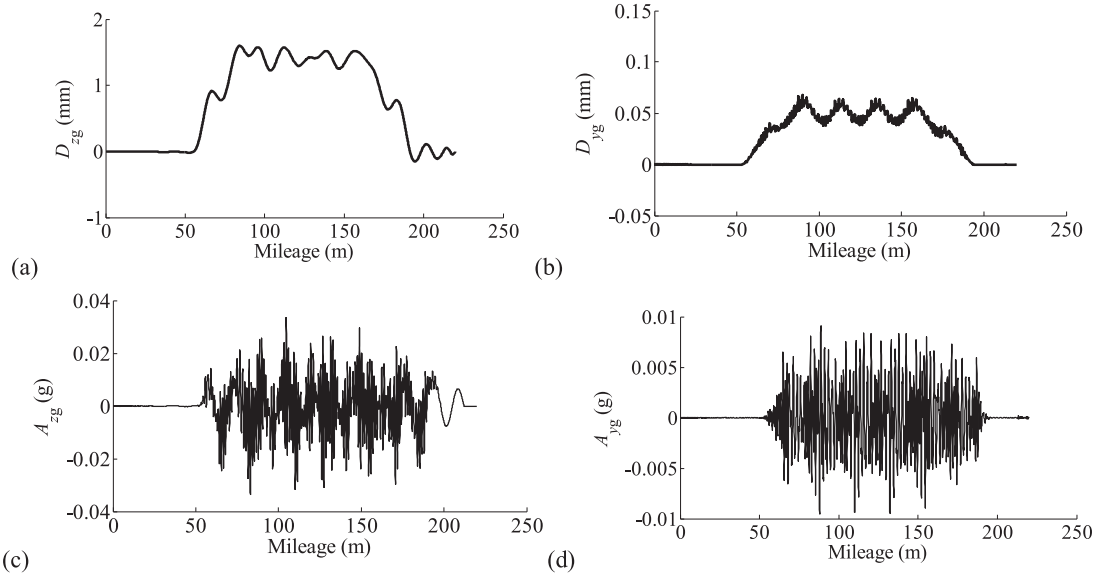

Fig. 7. The displacement and acceleration of the bridge at the mid-span (a. vertical displacement of the centroid of the bridge; b. lateral displacement with regard to the middle point of the track-bridge contact area; c. vertical acceleration of the centroid of the bridge; d. lateral acceleration with regard to the middle point of the track-bridge contact area).

status. With regarding to the acceleration of the bridge at the mid-span, the responses are generally zero-mean stationary processes controlled with the limits, i.e., 0.35 g for vertical acceleration and 0.14 g for lateral acceleration.

For investigating the influence of train speed on the system vibrations, the speed of the train is set to increase from 200 km/h to 800 km/h with an increment of 10 km/h. The vertical and lateral natural frequency of the bridge are respectively 8.91 Hz and 3.98 Hz. Fig. 8 shows the maximum responses of the wheel-rail force and the acceleration of the mid-span against different train speeds. It can be observed that the resonance speed of the train for the bridge vertical vibration is significantly larger than that for the bridge lateral vibration due to its higher natural frequency. Obviously it can be seen that the wheel-rail forces are generally promoted by the increase of the train speed, besides the resonance of the bridge will strengthen dynamical impacts on wheel-rail interactions on the basis of the moving of the train. See for instance, when the train speed reaches 710 km/h (resonant train speed), the wheel-rail vertical force is significantly enlarged, which also causes the fluctuation of the wheel-rail lateral force since the wheel-rail vertical/lateral interactions are coupled in 3-D space in the dynamical model.

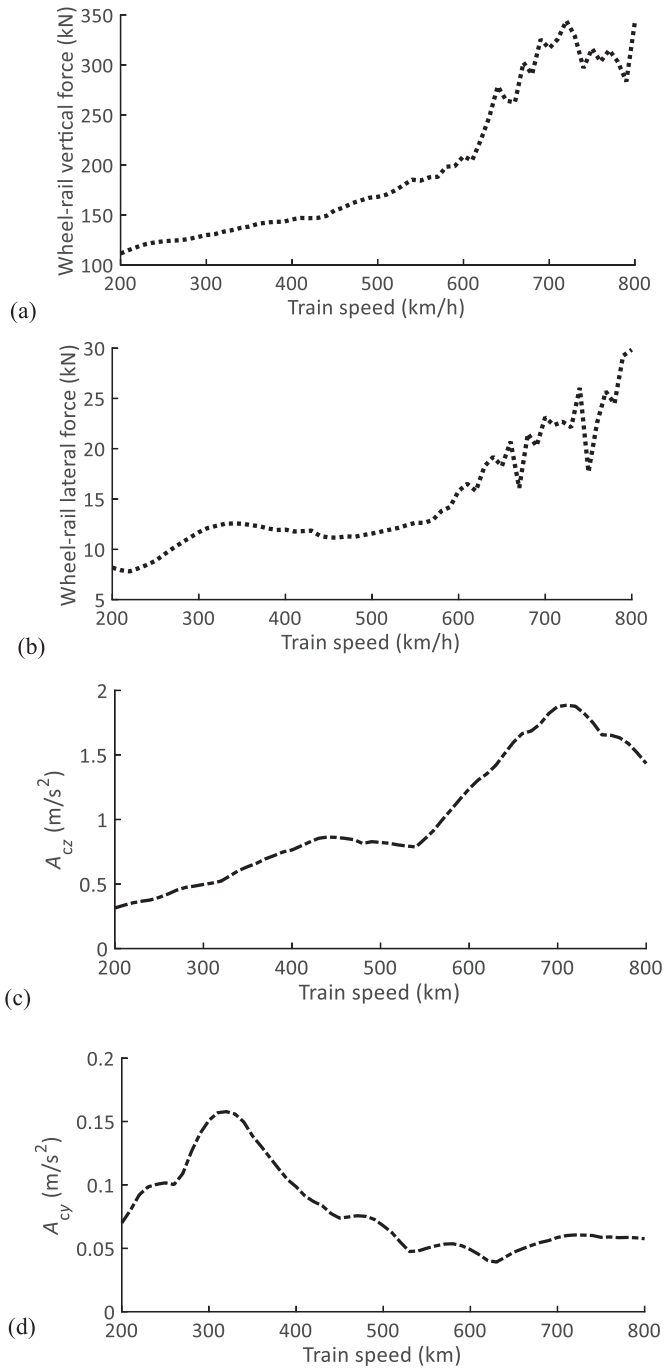

Fig. 8. Maximum dynamic responses against running speeds (a. wheel-rail vertical force; b. wheel-rail lateral force; c. vertical acceleration at the mid-span; lateral acceleration at the mid-span).

For the simply supported beam under moving loads, the resonant train speed V_g can be estimated by Xia et al. [37]

$$V_g = \frac{3.6 f_{gn} L_g}{i}, \quad n = 1, 2, ..., \quad i = 1, 2, ... \tag{55}$$

where f_{gn} is the nth vertical or lateral natural frequency of the bridge (Hz), L_g is the interval of the moving loads (m), $L_g = 22.125$ m in this example.

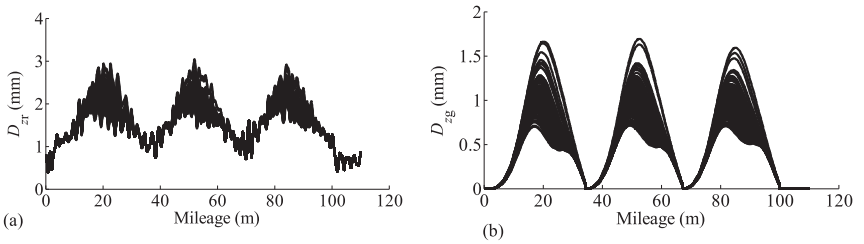

Fig. 9. Spatial deviation of response due to randomness of the girder parameters (a. rail vertical displacement; b. girder vertical displacement).

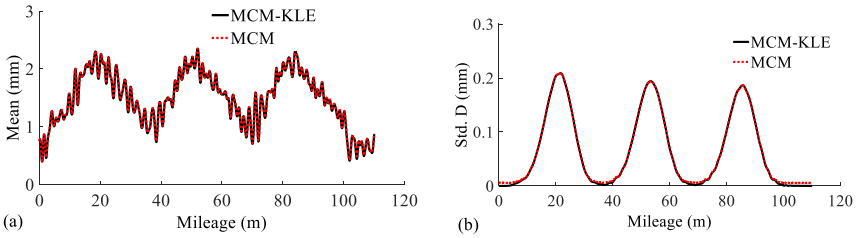

Fig. 10. Comparison between the statistical results of MCM-KLE and MCM with respect to the time-varying vertical displacement of the rail (a. mean; b. standard deviation).

Theoretically the resonant train speeds for the bridge vertical and lateral vibration are respectively 709 km/h and 317 km/h that are derived by Eq. (55). Obviously the resonant speeds obtained by the numerical computations coincide well with the theoretical ones.

5.2. Case 2: the influence of the spatial randomness of system parameters

In this study, we will put an emphasis on identifying the influence of structural randomness on the dynamic behaviors of train-track-bridge systems, in which the structural randomness is mainly characterized by the dynamic characteristics of the system parameters.

For investigating the dynamic effects of spatial randomness regarding various system structures [38], five computational conditions are classified, namely

- Spatial randomness of the rail. Random parameters: elastic modulus E_{r}, mass per unit length M_{r}, flexural moment of inertia about the y-axis I_{ry}, flexural moment of inertia about the z-axis I_{rz}, denoted by C_1;
- Spatial randomness of the rail pads. Random parameters: lateral and vertical stiffness coefficients $k_{\mathrm{rp},y}$ and $k_{\mathrm{rp},z}$, lateral and vertical damping coefficients $c_{\mathrm{rp},y}$ and $c_{\mathrm{rp},z}$, denoted by C_2;
- Spatial randomness of the CAM. Random parameters: lateral and vertical stiffness coefficients $k_{\mathrm{ca},y}$ and $k_{\mathrm{ca},z}$, lateral and vertical damping coefficients $c_{\mathrm{ca},y}$ and $c_{\mathrm{ca},z}$, denoted by C_3;
- Spatial randomness of the girder. Random parameters: lateral and vertical stiffness coefficients $k_{\mathrm{ca},y}$ and $k_{\mathrm{ca},z}$, lateral and vertical damping coefficients $c_{\mathrm{ca},y}$ and $c_{\mathrm{ca},z}$, denoted by C_4;

It is assumed that the random parameters are all following normal distribution with coefficients of variation of 0.1 and correlation coefficient of 0.7–0.9, for each computational condition. Besides, only a three span simply supported girder bridge is considered for advancing the efficiency of numerical analysis, and running speed of the vehicle is 300 km/h.

Fig. 9 shows the displacement deviations of the rail and the girder in C_4 condition, from which one can observe that the spatial randomness of the girder holds significant influence on structural vibrations; due to the variation of the girder parameters, the discrepancy between the minimum and maximum displacement may even hold a double difference.

Besides, to validate the effectiveness of the MCM-KLE method presented in Section 3.1, Fig. 10 illustrates the comparisons of statistical indices over time-varying vertical displacement of girder between the MCM-KLE with 174 samples and MCM with 2000 samples. As observed from Fig. 10, the results of these two methods are in agreement with each other well, but the MCM-KLE approach greatly reduces the time-consuming of computation.

Figs. 11–13 respectively show the dynamic effects of spatial randomness of system structural parameters on the lateral acceleration of the girder, the wheel-rail lateral force and the lateral acceleration of the car body. As seen from Figs. 11–13, the randomness of structure dynamic characteristics holds significant impacts on the variation of the system responses, because of the stationary feature of system excitations, the mean values are remained nearly unchanged across all variants. However, it can be derived from Figs. 11(b)–13 (b) that the degree of dynamic effects are significantly different against different dynamic indices when the structural components that shows random properties are different. See for example, the

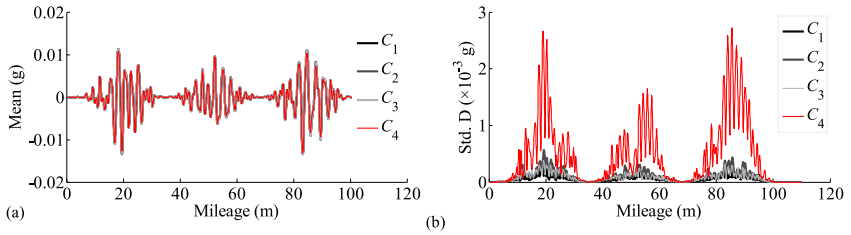

Fig. 11. The statistical results of the time-varying lateral acceleration of the girder under different system conditions (a. mean; b. standard deviation).

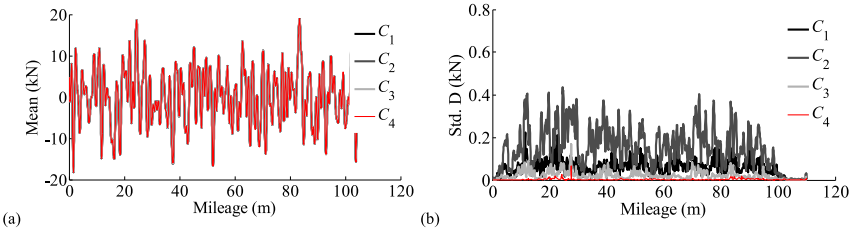

Fig. 12. The statistical results of the wheel-rail lateral force under different system conditions (a. mean; b. standard deviation.

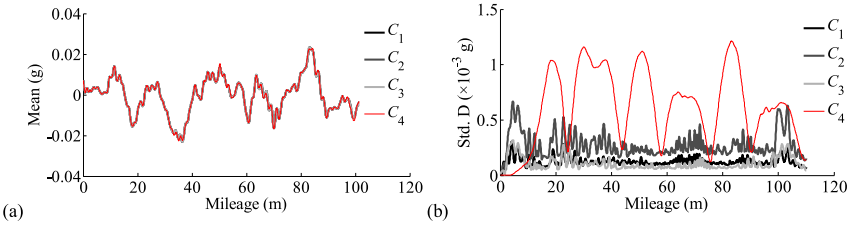

Fig. 13. The statistical results of the vertical acceleration of the car body under different system conditions (a. mean; b. standard deviation).

Table 1
Standard deviations for different dynamic indices with respect to spatial randomness of system parameters.

Dynamic indices	Computational conditions			
	C_1	C_2	C_3	C_4
A_{yr}	0.212	0.258	0.203	0.132
A_{zr}	0.300	0.238	0.115	0.017
A_{yg} ($\times 10^{-3}$ g)	0.400	0.600	0.400	2.700
A_{zg} ($\times 10^{-3}$ g)	0.900	2.300	3.200	6.900
A_{yc} ($\times 10^{-3}$ g)	0.147	0.3414	0.070	0.036
A_{zc} ($\times 10^{-3}$ g)	0.300	0.700	0.300	1.200
F_{yw} ($\times 10^{-3}$ kN)	0.224	0.436	0.168	0.066
F_{zw} (kN)	0.921	1.899	1.135	0.158

Note: A_{yr} - lateral acceleration of the rail; A_{zr} - vertical acceleration of the rail; A_{yg} - lateral acceleration of the girder; A_{zg} - vertical acceleration of the girder; A_{yc} - lateral acceleration of the car body; A_{zc} - vertical acceleration of the car body; F_{yw} - wheel-rail lateral force; F_{zw} - wheel-rail vertical force.

random characteristics of the bridge girder play a critical role in affecting the variations of the lateral acceleration of the girder, however, its influence on wheel-rail lateral force is relative small, instead, the variations of the dynamic parameters of the rail pads become the most important factor influencing the response magnitude of wheel-rail forces; moreover, Fig. 13(b) shows that the key factor affecting the variation of the vertical vibration of the car body is the randomness of the girder parameters, which might be a special phenomenon that only occurring on railway bridges, in normal railway sections, the random parameters of the subgrade tracks only bring about very small effects on vibrations of the car body.

Table 1 further lists the maximum standard deviations of dynamic indices with respect to various computation conditions, from which one can conveniently clarify the main structural components possessing the most significant impacts on the vibrations of a specific index.

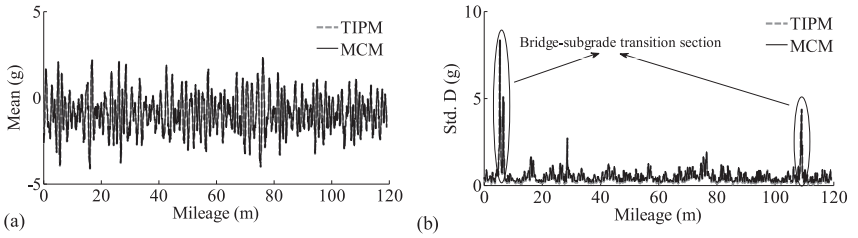

Fig. 14. Statistical comparisons between TIPM and MCM through rail vertical acceleration (a. mean value; b. standard deviation).

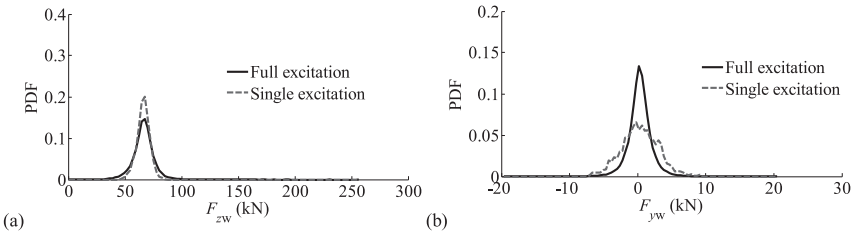

Fig. 15. PDF comparison between full excitation and single excitation (a. wheel-rail vertical force; b. wheel-rail lateral force).

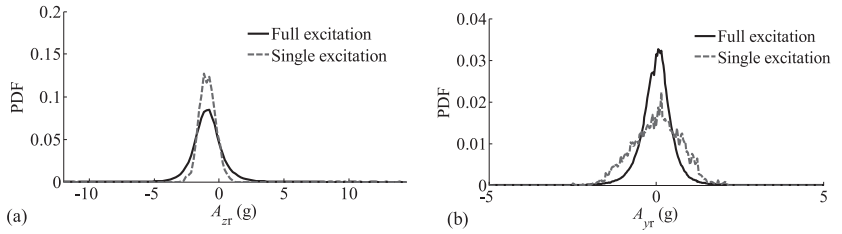

Fig. 16. PDF comparison between full excitation and single excitation (a. rail vertical acceleration; b. rail lateral acceleration).

5.3. Case 3: full excitation of track irregularities

In the previous section, track irregularities, as geometrical excitations of the rail profile, are set to be deterministic to afford a more clarity of the dynamic influence induced by the randomness of system parameters. However, as stated in the introduction, the track irregularities on the bridge tracks are random and variant in nature, especially in a situation with large-scale constructions of railway bridges.

In this example, a case for investigating the influence of the uncertainty of track irregularities on dynamical assessment of train-track-bridge systems is presented by introducing the track irregularity probabilistic model (TIPM), where the track irregularities are cumulatively collected from a high-speed line (Wuhan-Guangzhou) in three years with a detection interval of one month. Through TIPM, the dynamic response under full excitations of track irregularities can be obtained with a high efficiency.

To validate the effectiveness of TIPM, Monte-Carlo method (MCM) is applied to select the track irregularity sets adequately. Fig. 14 plots the comparison of statistical results between TIPM and MCM regarding rail vertical accelerations, from which one can observe that these two results coincide well with each other, however, 2999 samples are used in the MCM, which is greatly larger than that of TIPM, i.e., 304 samples. Besides, it can be noted that the variations of the acceleration will be enlarged by the abrupt change of track stiffness at bridge-subgrade transition sections.

By introducing TIPM, the full excitations due to track irregularities can be revealed, but in most researches, only a single excitation is loaded, in which a statistical average track irregularity set is used as the system excitation. Figs. 15 and 16 plot the probability density function (PDF) comparisons between full excitation and single excitation with specific to wheel-rail forces and rail accelerations, from which one can observed that there exists significant differences between results of these two forms of excitations no matter on maximum responses or on PDF distributions. Thus it can be deduced that whether to consider the full excitation of track irregularities will remarkably influence the results on aspects of reliability assessment and prediction of extremum.

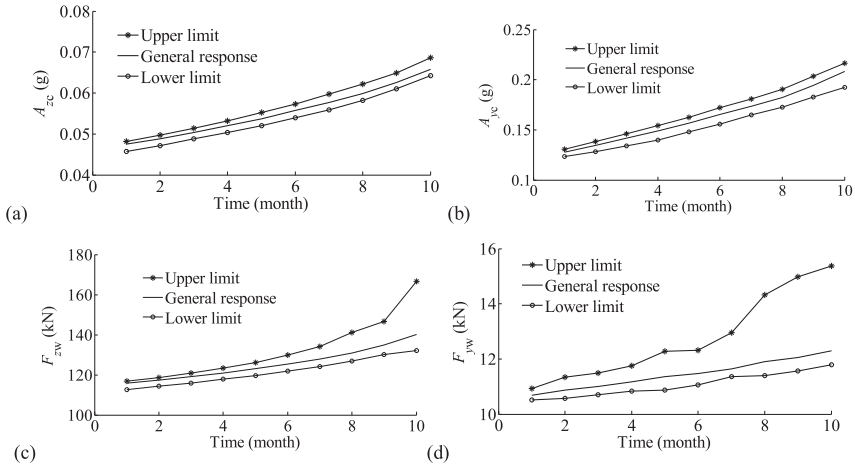

Fig. 17. Long-term behaviors of system responses (a. vertical acceleration at the mid-span; b. lateral acceleration at the mid-span; c, wheel-rail vertical force; d. wheel-rail lateral force).

5.4. Case 4: temporal prediction of system performance due to evolution of dynamic characteristics of systems

The spectral evolution method developed in Section 3.3 is validated to be fairly practical, which can be used to statistically reveal the time-evolving process of track irregularities, and having been reported in a key project of The National Natural Science Fund of China [39] with specific to the vehicle-track system.

Based on the spectral evolution method, predictions for the long-term behaviors of train-track-bridge systems can be estimated. The spectral densities of track irregularities $\boldsymbol{P}_{\varsigma}(\omega;\ t_{i+1})$ at time t_{i+1} can be clarified based on the power spectrum at time t_i, i.e., $\boldsymbol{P}_{\varsigma}(\omega;\ t_i)$ and an enlarge factor, i.e., $\tilde{p}_{\varsigma}(t_i)$, where $i=1, 2, ..., H$ and $[t_1,t_H]$ denotes the whole time period predicted, that is,

$$\boldsymbol{P}_{\varsigma}(\omega;t_{i+1}) = \boldsymbol{P}_{\varsigma}(\omega;t_i) + F^{-1}_{\varsigma,\omega}(\tilde{p}_{\varsigma}(t_i)) \tag{56}$$

where $\tilde{p}_{\varsigma}(t_i)$ is the cumulative probability that is statistically obtained to characterize the degree of evolution of the spectral densities, and then the domain of evolution spectrums $\boldsymbol{\Omega}_{\boldsymbol{P}'}(t_{i+2})$ over time period of $[t_{i+1},\ t_{i+2}]$ are confirmed by the spectral characteristics of $\boldsymbol{P}_{\varsigma}(\omega;\ t_{i+1})$.

Here, only representative results against the evolution of system characteristics are presented without further experimental verifications, through which the related methods can be extended to the long-term dynamics prediction of the train-track-bridge interactions in the same manner. As a numerical example, Fig. 17 plots the general, upper and lower limits of the vertical and lateral acceleration of the girder at the mid-span, the lateral acceleration of the car body, the wheel-rail vertical and lateral force, respectively. In Fig. 17, the upper and lower limits of the response are presented to define the influence of uncertainty of evolutions. As observed from Fig. 17, the system responses are generally increased by the cyclic operations of railway trains. However, it should be noted that this example is only regarding to a specific condition of track random irregularities and system parameter variations.

In practical usage, the system characteristic of train-track-bridge systems should be actually measured and then loaded into the dynamic model to obtain more realistic results.

6. Conclusions

With the sufficiency and perfection on deterministically computational and analytical theory and method, special attentions on how to achieve a systematic quantification of the dynamical effects aroused by the uncertainty have been paid in recent years. Due to inevitable error in construction, measurement and prediction, we naturally cannot obtain the exact solution for such a complex dynamic system like train-track-bridge interactions. In this paper, a systematic work aiming at train-track-bridge systems is conducted to fully probe into its randomness stemming from spatial deviations and temporal evolutions and revealing its random vibrations through a train-track-bridge interaction model.

Following the modelling framework and fundamentals of this work, the longitudinal heterogeneity, randomness and evolution of the system excitations can be effectively simulated with higher efficiency and accordingly, the full view of the system behaviors brought out by the uncertain factors can be revealed from aspects of response characteristics, random vibration, dynamic reliability and long-term prediction, etc.

Apart from the model validations, some conclusions can be drawn accordingly:

1) The longitudinal inhomogeneity of the bridge girder shows significant influence on girder's response deviations, especially on the car body accelerations, which is rather different from the dynamic characteristics caused by embankment supports. However its influence on wheel-rail force is slight.
2) The resonance effect of the bridge girder caused by the moving load series or the loading rate of the train has been revealed in this work. It can be observed from the results that the vibration of the bridge systems will be significantly amplified by the resonance, besides the wheel-rail forces are also prompted by the resonance effects except the train speed.
3) The PDF characterizations for system responses are rather different if the spectral excitation of track irregularity is deficiently considered, which subsequently affects the reliability assessment of this dynamical system.

Acknowledgement

This work was supported by the key project of National Natural Science Fund [51735012; 51478482; 51678507]; the program of Introducing Talents of Discipline to Universities (111 Project) [No. B16041]; the support of the China Scholarship Council.

Appendix A

Table A1, Table A2, Table A3

Table A1
The degrees of freedom (DOFs) for vehicle systems.

Vehicle components	DOFs				
	Transverse	Bounce	Yaw	Pitch	Roll
Car body	y_c	z_c	ψ_c	β_c	φ_c
Front bogie frame	y_{Gq}	z_{Gq}	ψ_{Gq}	β_{Gq}	φ_{Gq}
Rear bogie frame	y_{Gh}	z_{Gh}	ψ_{Gh}	β_{Gh}	φ_{Gh}
Wheelset, $i=1\sim4$	y_{wi}	z_{wi}	ψ_{wi}	β_{wi}	φ_{wi}

Table A2
The degrees of freedom (DOFs) for the rail element node.

DOFs type					
Linear displacement			Angular displacement		
Along *X*-axis	Along *Y*-axis	Along *Z*-axis	Around *X*-axis	Around *Y*-axis	Around *Z*-axis
x_r	y_r	z_r	θ_{rx}	θ_{ry}	θ_{rz}

Table A3
The degrees of freedom (DOFs) for the slab track.

Vibration type	Element node	DOFs type				
		Linear displacement		Angular displacement		
Vertical	$\boldsymbol{X}_{s,v,i}$, $i=1, 2, 3, 4$	–	z_s	θ_{sx}	θ_{sy}	–
Lateral	$\boldsymbol{X}_{s,L,i}$, $i=1, 2$	y_s	–	–	–	θ_{sz}

Appendix B [29]

$$\begin{aligned}\boldsymbol{K}_{Tr} = \boldsymbol{K}_{Mo} = {} & \boldsymbol{K}_{sz1}(\boldsymbol{\Theta}_{sz1}, \boldsymbol{\Theta}_{sz1}) + \boldsymbol{K}_{sz2}(\boldsymbol{\Theta}_{sz2}, \boldsymbol{\Theta}_{sz2}) + \boldsymbol{K}_{sy1}(\boldsymbol{\Theta}_{sy1}, \boldsymbol{\Theta}_{sy1}) + \boldsymbol{K}_{sy2}(\boldsymbol{\Theta}_{sy2}, \boldsymbol{\Theta}_{sy2}) + \boldsymbol{K}_{sx1}(\boldsymbol{\Theta}_{sx1}, \boldsymbol{\Theta}_{sx1}) \\ & + \boldsymbol{K}_{sx2}(\boldsymbol{\Theta}_{sx2}, \boldsymbol{\Theta}_{sx2}) + \boldsymbol{K}_{pz1}(\boldsymbol{\Theta}_{pz1}, \boldsymbol{\Theta}_{pz1}) + \boldsymbol{K}_{pz2}(\boldsymbol{\Theta}_{pz2}, \boldsymbol{\Theta}_{pz2}) + \boldsymbol{K}_{pz3}(\boldsymbol{\Theta}_{pz3}, \boldsymbol{\Theta}_{pz3}) + \boldsymbol{K}_{pz4}(\boldsymbol{\Theta}_{pz4}, \boldsymbol{\Theta}_{pz4}) \\ & + \boldsymbol{K}_{py1}(\boldsymbol{\Theta}_{py1}, \boldsymbol{\Theta}_{py1}) + \boldsymbol{K}_{py2}(\boldsymbol{\Theta}_{py2}, \boldsymbol{\Theta}_{py2}) + \boldsymbol{K}_{py3}(\boldsymbol{\Theta}_{py3}, \boldsymbol{\Theta}_{py4}) + \boldsymbol{K}_{py4}(\boldsymbol{\Theta}_{py4}, \boldsymbol{\Theta}_{py4}) \\ & + \boldsymbol{K}_{px1}(\boldsymbol{\Theta}_{px1}, \boldsymbol{\Theta}_{px1}) + \boldsymbol{K}_{px2}(\boldsymbol{\Theta}_{px2}, \boldsymbol{\Theta}_{px2}) + \boldsymbol{K}_{px3}(\boldsymbol{\Theta}_{px3}, \boldsymbol{\Theta}_{px4}) + \boldsymbol{K}_{px4}(\boldsymbol{\Theta}_{px4}, \boldsymbol{\Theta}_{px4})\end{aligned}$$

with

$$\begin{aligned}
&\boldsymbol{\Theta}_{sz1} = \begin{bmatrix} z_c & \phi_c & \beta_c & z_{Gq} & \phi_{Gq} \end{bmatrix},\ \boldsymbol{K}_{sz1}(\boldsymbol{\Theta}_{sz1}, \boldsymbol{\Theta}_{sz1}) = k_{sz}(\boldsymbol{N}_{sz1,1}^{T}\boldsymbol{N}_{sz1,1} + \boldsymbol{N}_{sz1,2}^{T}\boldsymbol{N}_{sz1,2});\\
&\boldsymbol{\Theta}_{sz2} = \begin{bmatrix} z_c & \phi_c & \beta_c & z_{Gh} & \phi_{Gh} \end{bmatrix},\ \boldsymbol{K}_{sz2}(\boldsymbol{\Theta}_{sz2}, \boldsymbol{\Theta}_{sz2}) = k_{sz}(\boldsymbol{N}_{sz2,1}^{T}\boldsymbol{N}_{sz2,1} + \boldsymbol{N}_{sz2,2}^{T}\boldsymbol{N}_{sz2,2});\\
&\boldsymbol{\Theta}_{sy1} = \begin{bmatrix} y_c & \phi_c & \psi_c & y_{Gq} & \phi_{Gq} \end{bmatrix},\ \boldsymbol{K}_{sy1}(\boldsymbol{\Theta}_{sy1}, \boldsymbol{\Theta}_{sy1}) = 2k_{sy}\boldsymbol{N}_{sy1}^{T}\boldsymbol{N}_{sy1};\\
&\boldsymbol{\Theta}_{sy2} = \begin{bmatrix} y_c & \phi_c & \psi_c & y_{Gh} & \phi_{Gh} \end{bmatrix},\ \boldsymbol{K}_{sy2}(\boldsymbol{\Theta}_{sy2}, \boldsymbol{\Theta}_{sy2}) = 2k_{sy}\boldsymbol{N}_{sy2}^{T}\boldsymbol{N}_{sy2};\\
&\boldsymbol{\Theta}_{sx1} = \begin{bmatrix} \psi_c & \psi_{Gq} & \beta_c & \beta_{Gq} \end{bmatrix},\ \boldsymbol{K}_{sx1}(\boldsymbol{\Theta}_{sx1}, \boldsymbol{\Theta}_{sx1}) = k_{sx}(\boldsymbol{N}_{sx1,1}^{T}\boldsymbol{N}_{sx1,1} + \boldsymbol{N}_{sx1,2}^{T}\boldsymbol{N}_{sx1,2});\\
&\boldsymbol{\Theta}_{sx2} = \begin{bmatrix} \psi_c & \psi_{Gh} & \beta_c & \beta_{Gh} \end{bmatrix},\quad \boldsymbol{K}_{sx2}(\boldsymbol{\Theta}_{sx2}, \boldsymbol{\Theta}_{sx2}) = k_{sx}(\boldsymbol{N}_{sx2,1}^{T}\boldsymbol{N}_{sx2,1} + \boldsymbol{N}_{sx2,2}^{T}\boldsymbol{N}_{sx2,2});\\
&\boldsymbol{\Theta}_{pz1} = [z_{Gq} \quad z_{w1} \quad \phi_{Gq} \quad \phi_{w1} \quad \beta_{Gq}],\quad \boldsymbol{K}_{pz1}(\boldsymbol{\Theta}_{pz1}, \boldsymbol{\Theta}_{pz1}) = k_{pz}(\boldsymbol{N}_{pz1,1}^{T}\boldsymbol{N}_{pz1,1} + \boldsymbol{N}_{pz1,2}^{T}\boldsymbol{N}_{pz1,2});\\
&\boldsymbol{\Theta}_{pz2} = [z_{Gq} \quad z_{w2} \quad \phi_{Gq} \quad \phi_{w2} \quad \beta_{Gq}],\quad \boldsymbol{K}_{pz2}(\boldsymbol{\Theta}_{pz2}, \boldsymbol{\Theta}_{pz2}) = k_{pz}(\boldsymbol{N}_{pz21}^{T}\boldsymbol{N}_{pz21} + \boldsymbol{N}_{pz2,2}^{T}\boldsymbol{N}_{pz2,2});\\
&\boldsymbol{\Theta}_{pz3} = [z_{Gh} \quad z_{w3} \quad \phi_{Gh} \quad \phi_{w3} \quad \beta_{Gh},\quad \boldsymbol{K}_{pz3}(\boldsymbol{\Theta}_{pz3}, \boldsymbol{\Theta}_{pz3}) = k_{pz}(\boldsymbol{N}_{pz31}^{T}\boldsymbol{N}_{pz31} + \boldsymbol{N}_{pz3,2}^{T}\boldsymbol{N}_{pz3,2});\\
&\boldsymbol{\Theta}_{pz4} = [z_{Gh} \quad z_{w4} \quad \phi_{Gh} \quad \phi_{w4} \quad \beta_{Gh}],\quad \boldsymbol{K}_{pz4}(\boldsymbol{\Theta}_{pz4}, \boldsymbol{\Theta}_{pz4}) = k_{pz}(\boldsymbol{N}_{pz41}^{T}\boldsymbol{N}_{pz41} + \boldsymbol{N}_{pz4,2}^{T}\boldsymbol{N}_{pz4,2});\\
&\boldsymbol{\Theta}_{py1} = [y_{Gq} \quad y_{w1} \quad \phi_{Gq} \quad \psi_{Gq}],\quad \boldsymbol{K}_{py1}(\boldsymbol{\Theta}_{py1}, \boldsymbol{\Theta}_{py1}) = 2k_{py}\boldsymbol{N}_{py1}^{T}\boldsymbol{N}_{py1};\\
&\boldsymbol{\Theta}_{py2} = [y_{Gq} \quad y_{w2} \quad \phi_{Gq} \quad \psi_{Gq}],\quad \boldsymbol{K}_{py2}(\boldsymbol{\Theta}_{py2}, \boldsymbol{\Theta}_{py2}) = 2k_{py}\boldsymbol{N}_{py2}^{T}\boldsymbol{N}_{py2};\\
&\boldsymbol{\Theta}_{py3} = [y_{Gh} \quad y_{w3} \quad \phi_{Gh} \quad \psi_{Gh}],\quad \boldsymbol{K}_{py3}(\boldsymbol{\Theta}_{py3}, \boldsymbol{\Theta}_{py3}) = 2k_{py}\boldsymbol{N}_{py3}^{T}\boldsymbol{N}_{py3};\\
&\boldsymbol{\Theta}_{py4} = [y_{Gh} \quad y_{w4} \quad \phi_{Gh} \quad \psi_{Gh}],\quad \boldsymbol{K}_{py4}(\boldsymbol{\Theta}_{py4}, \boldsymbol{\Theta}_{py4}) = 2k_{py}\boldsymbol{N}_{py4}^{T}\boldsymbol{N}_{py4};\\
&\boldsymbol{\Theta}_{px1} = [\psi_{Gq} \quad \psi_{w1} \quad \beta_{Gq}],\quad \boldsymbol{K}_{px1}(\boldsymbol{\Theta}_{px1}, \boldsymbol{\Theta}_{px1}) = k_{px}(\boldsymbol{N}_{px1,1}^{T}\boldsymbol{N}_{px1,1} + \boldsymbol{N}_{px1,2}^{T}\boldsymbol{N}_{px1,2});\\
&\boldsymbol{\Theta}_{px2} = [\psi_{Gq} \quad \psi_{w2} \quad \beta_{Gq}],\quad \boldsymbol{K}_{px2}(\boldsymbol{\Theta}_{px2}, \boldsymbol{\Theta}_{px2}) = k_{px}(\boldsymbol{N}_{px21}^{T}\boldsymbol{N}_{px21} + \boldsymbol{N}_{px2,2}^{T}\boldsymbol{N}_{px2,2});\\
&\boldsymbol{\Theta}_{px3} = [\psi_{Gh} \quad \psi_{w3} \quad \beta_{Gh}],\quad \boldsymbol{K}_{px3}(\boldsymbol{\Theta}_{px3}, \boldsymbol{\Theta}_{px3}) = k_{px}(\boldsymbol{N}_{px31}^{T}\boldsymbol{N}_{px31} + \boldsymbol{N}_{px3,2}^{T}\boldsymbol{N}_{px3,2});\\
&\boldsymbol{\Theta}_{px4} = [\psi_{Gh} \quad \psi_{w4} \quad \beta_{Gh}],\quad \boldsymbol{K}_{px4}(\boldsymbol{\Theta}_{px4}, \boldsymbol{\Theta}_{px4}) = k_{px}(\boldsymbol{N}_{px41}^{T}\boldsymbol{N}_{px41} + \boldsymbol{N}_{px4,2}^{T}\boldsymbol{N}_{px4,2}),
\end{aligned}$$

in which $\boldsymbol{K}_{sz1}$, $\boldsymbol{K}_{sy1}$ and $\boldsymbol{K}_{sx1}$ denote the stiffness matrices derived by the interactions between the car body and the front bogie frame in vertical, lateral and longitudinal directions; $\boldsymbol{K}_{sz2}$, $\boldsymbol{K}_{sy2}$ and $\boldsymbol{K}_{sx2}$ denote the stiffness matrices derived by the interactions between the car body and the rear bogie frame in vertical, lateral and longitudinal directions; $\boldsymbol{K}_{pz1}$, $\boldsymbol{K}_{pz2}$, $\boldsymbol{K}_{pz3}$ and $\boldsymbol{K}_{pz4}$ denote the stiffness matrices derived by the interactions between the bogie frame and the 1st and 2nd wheelset and the interactions between the rear bogie frame and the 3rd and 4th wheelset in vertical direction; $\boldsymbol{K}_{py1}$, $\boldsymbol{K}_{py2}$, $\boldsymbol{K}_{py3}$ and $\boldsymbol{K}_{py4}$ denote the stiffness matrices derived by the interactions between the bogie frame and the 1st and 2nd wheelset and the interactions between the rear bogie frame and the 3rd and 4th wheelset in lateral direction; $\boldsymbol{K}_{px1}$, $\boldsymbol{K}_{px2}$, $\boldsymbol{K}_{px3}$ and $\boldsymbol{K}_{px4}$ denote the stiffness matrices derived by the interactions between the bogie frame and the 1st and 2nd wheelset and the interactions between the rear bogie frame and the 3rd and 4th wheelset in longitudinal direction; moreover, $\boldsymbol{N}_{sz}$, $\boldsymbol{N}_{sy}$ and $\boldsymbol{N}_{sx}$ denote the equivalent shape functions used to characterize the relative motions between DOFs, whose detailed expressions are shown below:

$$\begin{aligned}
&\boldsymbol{N}_{sz1,1} = [1 \quad -d_s \quad -l_c \quad -1 \quad d_s], && \boldsymbol{N}_{sz1,2} = [1 \quad d_s \quad -l_c \quad -1 \quad -d_s],\\
&\boldsymbol{N}_{sz2,1} = [1 \quad -d_s \quad l_c \quad -1 \quad d_s], && \boldsymbol{N}_{sz2,2} = [1 \quad d_s \quad l_c \quad -1 \quad -d_s];\\
&\boldsymbol{N}_{sy1} = [-1 \quad -H_{cb} \quad -l_c \quad 1 \quad H_{bt}], && \boldsymbol{N}_{sy2} = [-1 \quad H_{cb} \quad l_c \quad 1 \quad H_{bt}];\\
&\boldsymbol{N}_{sx1,1} = [d_s \quad -d_s \quad H_{cb} \quad H_{bt}], && \boldsymbol{N}_{sx1,2} = [-d_s \quad d_s \quad H_{cb} \quad H_{bt}],\\
&\boldsymbol{N}_{sx2,1} = [d_s \quad -d_s \quad H_{cb} \quad H_{bt}], && \boldsymbol{N}_{sx2,2} = [-d_s \quad d_s \quad H_{cb} \quad H_{bt}];\\
&\boldsymbol{N}_{pz1,1} = [1 \quad -1 \quad -d_p \quad d_p \quad l_t], && \boldsymbol{N}_{pz1,2} = [1 \quad -1 \quad d_p \quad -d_p \quad -l_t],\\
&\boldsymbol{N}_{pz2,1} = [1 \quad -1 \quad -d_p \quad d_p \quad l_t], && \boldsymbol{N}_{pz2,2} = [1 \quad -1 \quad d_p \quad -d_p \quad l_t],\\
&N_{pz3,1} = N_{pz1,1}, \quad N_{pz3,2} = N_{pz1,2}, && N_{pz4,1} = N_{pz2,1}, \quad N_{pz4,2} = N_{pz2,2};\\
&\boldsymbol{N}_{py1} = [-1 \quad 1 \quad H_{tw} \quad -l_t], && \boldsymbol{N}_{py22} = [-1 \quad 1 \quad H_{tw} \quad l_t],\\
&N_{py3} = N_{py1}, \quad N_{py4} = N_{py2}; &&\\
&\boldsymbol{N}_{px1,1} = [d_p \quad -d_p \quad H_{tw}], && \boldsymbol{N}_{px1,2} = [-d_p \quad d_p \quad H_{tw}],\\
&N_{px2,1} = N_{px1,1}, \quad N_{px2,2} = N_{px1,2}, && N_{px3,1} = N_{px1,1}, \quad N_{px3,2} = N_{px1,2},\\
&N_{px4,1} = N_{px1,1}, \quad N_{px4,2} = N_{px1,2}, &&
\end{aligned}$$

References

[1] Y.B. Yang, C.H. Chang, J.D. Yau, An element for analyzing vehicle-bridge systems considering vehicle's pitching effect, Int. J. Numer. Method Eng. 46 (1999) 1031–1047.
[2] F.T.K Au, Y.S. Cheng, Y.K. Cheung, Effects of random road surface roughness and long-term deflection of prestressed concrete girder and cable-stayed bridge on impact due to moving vehicles, Comput. Struct. 79 (2001) 853–872.
[3] P. Lou, Z.W. Yu, F.T.K. Au, Rail-bridge coupling element of unequal lengths for analyzing train-track-bridge interaction systems, Appl. Math. Model. 36 (2012) 1395–1414.
[4] Y.Q. Sun, M. Dhanasekar, A dynamic model for the vertical interaction of the rail track and wagon system, Int. J. Solids Struct. 39 (2002) 1337–1359.
[5] O. Coussy, M. Said, J.P. Vanhoove, The influence of random surface irregularities on the dynamic response of bridges under suspended moving loads, J. Sound Vibr. 130 (1989) 313–320.
[6] J.M. Rocha, A.A. Henriques, R. Cal çada, Probabilistic safety assessment of a short span high-speed railway bridge, Eng. Struct. 71 (2014) 99–111.
[7] W.M. Zhai, X. Sun, A detailed model for investigating vertical interactions between railway vehicle and track, Veh. Syst. Dyn. 23 (1994) 603–615.
[8] Rådesctröm Sarah, Ülker-Kaustell Mahir, Andreas Andersson, Viktor Tell, Raid Karoumi, Application of fluid viscous dampers to mitigate vibrations of high-speed railway bridges, Int. J. Rail Transp. 5 (1) (2017) 47–62.
[9] W.M. Zhai, Chengbiao Cai, Kaiyun Wang, Fundamentals of vehicle-track coupled dynamics, Veh. Syst. Dyn. 47 (11) (2009) 1349–1376.
[10] W.M. Zhai, H. Xia, C.B. Cai, et al., High-speed train-track-bridge dynamic interactions-Part I: theoretical model and numerical simulation, Int. J. Rail Transp. 1 (1,2) (2013) 3–24.
[11] W.M. Zhai, C.B. Cai, Train/track/bridge dynamic interaction: simulation and applications, Veh. Syst. Dyn. 37 (2002) 653–665.
[12] M.H. Bhatti, V.K. Garg, K.H. Chu, Dynamic interaction between freight train and steel bridge, J. Dyn. Syst-T ASCE 107 (1985) 60–66.
[13] H. Xia, L.Y. Xu, T.H.T. Chan, Dynamic interaction of long suspension bridges with running trains, J. Sound Vibr. 237 (2000) 263–280.
[14] Y.S. Wu, Y.B. Yang, J.D. Yau, Three-dimensional analysis of train-rail-bridge interaction problems, Veh. Syst. Dyn. 36 (2001) 1–35.
[15] M.K. Song, H.C. Noh, C.K. Choi, A new three-dimensional finite element analysis model of high speed train-bridge interaction, Eng. Struct. 25 (2003) 1611–1626.
[16] Zhi-wu Yu, Jian-feng Mao, Feng-qi Guo, Wei Guo, Non-stationary random vibrations analysis of a 3-D train-bridge system using the probability density evolution method, J. Sound Vibr. 366 (2016) 173–189.
[17] X.H. He, Y.B. Gai, T. Wu, Simulation of train–bridge interaction under wind loads: a rigid-flexible coupling approach, Int. J. Rail Transp. 6 (3) (2018) 163–182.
[18] Zhi-Ping Zeng, Fu-Shan Liu, Ping Lou, Yan-Gang Zhao, Li-Min Peng, Formulation of three-dimensional equations of motion for train-slab track-bridge interaction system and its application to random vibration analysis, Appl. Math. Model. 40 (2016) 5891–5929.
[19] Q.Y. Zeng, P. Lou, J. Xiang, The principle of total potential energy with stationary value in elastic system dynamics and its application to the analysis of vibration and dynamic stability, J. Huazhong Univ. Sci. Tech. (Urban Sci. Ed.) 19 (1) (2002) 7–14.
[20] F.T.K. Au, J.J. Wang, Y.K. Cheung, Impact study of cable-stayed railway bridge with random rail irregularities, Eng. Struct. 24 (2002) 529–541.
[21] H. Xia, N. Zhang, Dynamic Interaction of Vehicles and Structures, Science Press, Beijing, 2005 (in Chinese).
[22] J.H. Lin, W.S. Zhang, J.J. Li., Structural responses to arbitrarily coherent stationary random excitation, Comput. Struct 50 (1994) 629–633.
[23] J.H. Lin, W.S. Zhang, F.W. Williams, Pseudo-excitation algorithm for non-stationary random seismic responses, Eng. Struct. 16 (1994) 270–276.
[24] Lei Xu, Wanming Zhai, Stochastic analysis model for vehicle-track coupled systems subject to earthquakes and track random irregularities, J. Sound Vibr. 407 (2017) 209–225.
[25] M. Mehrali, S. Mohammadzadeh, M. Esmaeili, M. Nouri, Investigating vehicle-slab track interaction considering random track bed stiffness, Sci. Iran. A 21 (1) (2014) 82–90.
[26] Lei Xu, Wanming Zhai, A new model for temporal-spatial stochastic analysis of vehicle-track coupled systems, Veh. Syst. Dyn. 55 (3) (2017) 427–448.
[27] Z.B. Jin, G.Q. Li, S.L. Pei, H.Y. Liu, Vehicle-induced random vibration of railway bridges: a spectral approach, Int. J. Rail Transp. 5 (4) (2017) 191–212.
[28] Lei Xu, Xianmai Chen, Xuwei Li, Xianglin He, Development of a railway wagon-track interaction model: case studies on excited tracks, Mech. Syst. Signal Process. 100 (2018) 877–898.
[29] Lei Xu, Wanming Zhai, Jianmin Gao, Global sensitivity analysis for vehicle-track interactions: special attentions on track irregularities, J. Comput. Nonlinear Dyn. 13 (2018) 031007.
[30] G. Chen, W.M. Zhai, A new wheel/rail spatially dynamic coupling model and its verification, Veh. Syst. Dyn. 41 (4) (2004) 301–322.
[31] S.T. Li, J.L. Hammond, Generation of pseudorandom numbers with specified univariate distributions and correlation coefficients, IEEE Trans. Syst. Man Cybernet. SMC 5 (5) (1975) 557–561.
[32] D.Z. Wen, R.H. Zhuo, D.J. Ding, H. Zheng, J. Cheng, Z.H. Li, Generation of correlated pseudorandom variables in Monte Carlo simulation, Acta Phys. Sin. 61 (2012) 1–8.
[33] M. Loève, Probability Theory, Fourth ed., Springer-Verlag, New York, 1977.
[34] R. Ghanem, P.D. Spanos, Spectral Methods for Uncertainty Quantification, Springer, 2010.
[35] KnioO Le Ma ître O, Spectral Methods for Uncertainty Quantification, Springer, 2010.
[36] L. Xu, W.M. Zhai, J.M. Gao, A probabilistic model for track random irregularities in vehicle/track coupled dynamics, Appl. Math. Model. 51 (2017) 145–158.
[37] H. Xia, N. Zhang, W.W. Guo, Analysis of resonance mechanism and conditions of train-bridge system, J. Sound Vibr. 297 (2006) 810–822.
[38] R.D. Frohling, H. Scheffel, W. EbersÖhn, The vertical dynamic response of a rail vehicle caused by track stiffness variations along the track, Veh. Syst. Dyn. 25 (1996) 175–187.
[39] National Basic Research Program of China ("973" Project), Basic researches on dynamic performance evolution of the high-speed railway infrastructure and its service safety, Grant No. 2013CB036200, Chengdu, 2013~2017.